AN INVESTIGATION OF THE EARTH'S FREE OSCILLATIONS

Thesis by

Stewart Wilson Smith

In Partial Fulfillment of the Requirements

For the Degree of

Doctor of Philosophy

California Institute of Technology

Pasadena, California

May 1961

ACKNOWLEDGMENTS

The author is indebted to Professors Frank Press and Hugo Benioff for their continued support and guidance throughout this study.

In the initial stages of this work, the data reduction and computing facilities of the Sandia Corporation were made available through the courtesy of Dr. C. F. Quate. It is a pleasure to acknowledge this assistance and also the valuable discussions held with Drs. B. Bogert and L. Koopmans while the author was at the Sandia Corporation.

Much of the subsequent computation was performed on IBM 7090 computers at the Western Data Processing Center located at U.C.L.A. and at the Jet Propulsion Laboratory of the California Institute of Technology.

This research was partially supported by contracts No. AF-49(638)910 and NAS w-81. During the period of this research the author held a Standard Oil Company of California Fellowship in Earth Sciences, and this support is gratefully acknowledged.

Most of the figures were prepared by Mr. Laszlo Lenches and the author wishes to extend special thanks to him for his assistance.

ABSTRACT

The free oscillations of the earth excited by the Chilean earthquake of 1960 have been measured by power spectral analysis of strain and pendulum seismographs. A revised and more precise table of free oscillation periods is presented. The period of the fundamental spheroidal mode ${}_0S_2^0$ is 53.82 minutes.

Fine structure analysis has shown that for the first three spheroidal modes there is good agreement between the observed splitting and that calculated for a rotating earth. Results for the toroidal modes are uncertain.

A theory is presented that allows recovery of some of the source properties from observations of phase differences for spheroidal modes. A comparison of theory with observation confirms original estimates of a fault length of 1000 km and a rupture velocity of between 3 and 4 km/sec. The effect of a moving source that decays exponentially with distance changes the pattern of phase shifts slightly but does not change estimates of the fault parameters. An alternative interpretation of the source properties in terms of the relative amplitudes of the $2n + 1$ split lines for each mode is presented but no calculations are performed.

Preliminary data on the effects of geomagnetic storms on the oscillations of the earth place an upper limit of about 5×10^{16} ergs/cph for the energy density associated with the elastic coupling of several magnetic storms.

TABLE OF CONTENTS

LIST OF TABLES

I. INTRODUCTION

The free oscillations of the earth have been discussed by theoreticians since the latter part of the 19th Century. The model of the earth used in their mathematical analyses has steadily increased in complexity from the homogeneous non-gravitating sphere of Lamb (1882) to a rotating, non-homogeneous layered earth complete with a liquid core and a solid inner core which is presently being investigated.

In contrast to the long history of theoretical work, the attempts to measure the free periods of the earth have all taken place in recent years. In 1954 Benioff proposed that a 57 minute periodicity visible on the strain records of the Kamchatka earthquake was the fundamental spheroidal mode of the earth, which at that time was thought to have a period of about 60 minutes. The low Q of this oscillation, and the fact that other modes were not visible with comparable amplitudes cast much doubt on its identification, however this observation renewed a great theoretical interest in the problem. Benioff, Harrison, La Coste, Munk, and Slichter (1959) attempted to measure free oscillations in the background noise of strain and gravimeter records using power spectral analysis. Their results were negative, but they established an upper limit for oscillations of the earth excited by continuing natural processes. Their sample did not include an earthquake disturbance. Press (1960) performed Fourier analysis of the Kamchatka earthquake, and although he did not succeed in observing the lower modes, the higher modes were present in his results. The theoretical values for their periods had not yet been computed however, so he was unable

to identify these higher modes. In 1959 a network was added to the Isabella strain seismometer which reduced the effect of the earth tide and permitted higher magnification. The Chilean earthquake of 1960 was the first great earthquake to be recorded on this new system, and it was from these records that we obtained our first experimentally determined values for the free periods of the earth.

Analysis of the Isabella and $\tilde{N}an\tilde{a}$ strain records was carried out during the summer of 1960 with the aid of the data reduction facilities of the Sandia Corporation. The results were conclusive enough by August of 1960 for the observed periods of 18 spheroidal and 5 toroidal modes to be reported on by Press, Benioff, and Smith at the I. U. G. G. meetings in Helsinki. At the same time, records of the La Coste Romberg gravimeter at U. C. L. A. were being analyzed by Ness (1961). Excellent agreement on the periods of spheroidal modes recorded by these two instruments added a great deal to the confidence we placed in these early results. After the announcement of these observations, Pekeris (1961) computed the theoretical periods for the higher order modes for several earth models, and for the first time we could use the natural periods of the earth as criteria to determine which earth model was most correct. Subsequently Alsop, Sutton, and Ewing (1961), Bogert (1961), and Buchheim (1961) were able to observe these modes in the records of their instruments.

The ability to measure the earth's free oscillations should bring to the field of geophysics a new and powerful tool for the investigation of the internal structure of the earth. It should be pointed out however,

that to this point there has been little new discovered about the earth's interior using this information, other than that our models of the earth from seismic data are correct to first order. A notable contribution along this line has been made by MacDonald and Ness (1961) using the toroidal periods only. The full power of this new information cannot be utilized until the combined data on toroidal, spheroidal, and radial modes can be used to refine our present earth models.

These observations have provided a new way of studying the source mechanism of earthquakes, and thus may lead to a better understanding of the stress distribution in crust and mantle.

II. METHODS OF ANALYSIS

Analog to Digital Conversion

In our initial study, records were digitized with a Telecomputing Corporation Telereader, recording both time and amplitude at non-equally spaced time increments directly on punched cards. The readings were made close enough so that the curve was approximately linear between points. These values were used to compute the values at equal time increments by linear interpolation, and the result was used as input to a Share program (CSTUKS) for power spectral analysis on an IBM 704. This data reduction and analysis was carried out with the cooperation of the Sandia Corporation, Albuquerque, New Mexico.

Subsequent digitizing has been accomplished by reading the records directly at equal time intervals on a Century Geophysical Corporation analog to digital converter. The chart paper is rolled across a viewing area at a rate controlled by an operator who follows the trace with a cross-hair. A counter is connected to the drum drive which records the position of the cross-hair at specified increments of drum rotation. The output of this system is a punched paper tape and an auxilliary recording of the digital values plotted on a strip chart recorder. This auxilliary recording is essential to check for large errors that might be present on the tape due to malfunctioning of the system, and also to check on the accuracy of the operator. For an extremely tangled seismogram, the auxiliary recording gives us an additional check on whether we have untangled the traces correctly. These tapes can be in an arbitrary 4 bit BCD format, or in the special

BCD format required by a Bendix G-15 computer, both of which can be easily converted to IBM cards. We find that paper tape used as an intermediate data storage medium plus card input controlled by Fortran subroutines to be a very flexible and convenient system for handling relatively large amounts of data.

Numerical Spectral Analysis

Two fundamental problems in numerical spectral analysis arise from the necessity of dealing with finite length records and with data that is sampled at discrete intervals. These two situations can be thought of as the result of operations performed on an infinite, continuous time record. The advantage of this view is that the effect of the corresponding operation in the frequency domain can be easily visualized. The operation of selecting a length of record might be multiplication of the time function by a "box car"

$$D(t) = 1 \quad \text{for} \quad |t| \leq T$$

$$= 0 \qquad\quad |t| > T$$

The Fourier transform of this function is

$$W(f) = (\sin \pi f T)/\pi f$$

and the corresponding operation in the frequency domain would be the convolution of $W(f)$ with the true spectrum. The fact that we can compute only a spectrum which is the convolution of the true spectrum with another function has been likened to looking at the spectrum through a

window, hence the term "spectral window" is used for the function $W(f)$.

A desirable spectral window will have a maximum at $f = 0$, will fall off steeply to zero at some frequency f_o and oscillate with only small amplitude from that point on. It will of course be symmetric about $f = 0$. The region between 0 and f_o is known as the "main beam," and the oscillations as "side lobes" by analogy with an antenna radiation pattern. The width of the main beam determines the resolution with which we can separate closely spaced spectral lines, and the height of the side lobes determines how much contamination there will be due to power in adjacent frequency bands.

A number of different window are in current use, and a comparison of their properties has been given by Parzen (1960). We have used the following time window in our power spectrum calculations:

$$D(t) = (1 + \cos \pi t/T)/2T \qquad |t| \leq T$$

$$= 0 \qquad |t| > T$$

with frequency response

$$W(f) = \frac{\sin 2\pi fT}{(1 - 4f^2T^2)2\pi fT}$$

The use of this window in power spectral analysis is particularly convenient because its multiplication times the covariance function is equivalent to smoothing the Fourier cosine series coefficients with the weights 1/4, 1/2, 1/4. This operation, known as "hanning" is discussed by Blackman and Tukey (1959).

In our fine structure analysis where we compute the Fourier

transform at arbitrary frequency increments, it is necessary to actually multiply the data by a time window rather than to perform a smoothing operation in the frequency domain. The window we have chosen for this type of analysis was suggested by Parzen (1960), and is shown in fig. 1. Its properties of beam width and side lobe height are better than the hanning window. The Parzen time window is given by

$$D(t) = 1 - 6\left|\frac{t}{T}\right|^2 + 6\left|\frac{t}{T}\right|^3 \qquad \left|\frac{t}{T}\right| \leq 1/2$$

$$D(t) = \left(1 - \left|\frac{t}{T}\right|\right)^2 \qquad 1/2 < \left|\frac{t}{T}\right| \leq 1$$

$$D(t) = 0 \qquad \left|\frac{t}{T}\right| > 1$$

with a frequency response

$$W(f) = \frac{3\sqrt{6}}{4}\left[\frac{\sin fT\sqrt{6}}{fT\sqrt{6}}\right]^4$$

We use this window because it is purely algebraic, easy to apply, all the side lobes are positive, and the first side lobe which is the largest is less than 0.2% of the peak height. For the extremely long records we have analyzed, the frequency resolution of this window has been more than adequate.

A Tchebycheff window can be constructed by equating a Tchebycheff polynomial of order n to a Fourier series of n terms and evaluating the coefficients. This has been described by Dolph (1946) and was used by Ness (1961). Dolph proved that the resulting function is optimum in the sense that it has the narrowest main beam for a given

side lobe height and the lowest side lobe height for a given beam width of any window with the same number of coefficients. We have not found it necessary to use such a window in our work.

The operation of sampling the data at discrete intervals Δt can be considered as multiplication of the continuous function by the periodic function

$$S(t) = 1 \quad \text{for} \quad n\Delta t, \quad \text{where} \quad n \quad \text{is an integer}$$

$$= 0 \quad \text{elsewhere}$$

The Fourier series expansion of this function is

$$S(t) = \sum_{-\infty}^{+\infty} C_k e^{2\pi i k t/\Delta t}$$

The sampled time function is then

$$F_s(t) = F(t) \cdot S(t)$$

$$= \sum_{-\infty}^{+\infty} C_k F(t) e^{2\pi i k t/\Delta t}$$

From this we see that if the true spectrum is $G(f)$, then by the shifting theorem the sampled spectrum will be

$$G_s(f) = \sum_{-\infty}^{+\infty} C_k G(f - k/\Delta t)$$

Thus the simple operation of sampling the continuous time function changes the spectrum into a periodic function, and irrevocably mixes up the frequencies f and $f \pm n/\Delta t$. These indistinguishable frequencies

are known as aliases. Aliasing can be visualized by folding the frequency axis like an accordian, with the folds at the points $n/2\Delta t$. When this folding has been completed one can see how the entire spectrum is distributed between the frequencies 0 and $1/2\Delta t$. The latter is sometimes referred to as the folding frequency.

Digital Filtering

In the preceding section it was pointed out that the computed value of the spectrum at a certain frequency contains contributions from other frequencies due to the effects of finite record length and discretely sampled data. This extraneous power can be reduced by proper filtering. There is of course no way to reduce the effect of aliasing introduced in the original digitizing of the analog record, so an adequate low pass electrical filter is essential in the recording system. When it is desired to reduce the original sampling rate, either for convenience or for computational speed, a digital low pass filter and decimation operation can be performed. A filtering operation in the time domain would be a convolution with a certain set of coefficients. These coefficients can be computed to give almost any desired filter response, see for instance Tukey (1959, p. 100). The sharpness of a cut-off will depend on the number of coefficients used. Decimation by N means to select every Nth point from the series. The effect in the frequency domain is division of the folding frequency by N. An ideal low pass and decimation operation would involve a filter that dropped to zero response for all frequencies greater than $1/2N\Delta t$, then when the spectrum is folded back by decimating by N, no new aliasing would be introduced.

We have used a symmetric low pass filter whose coefficients are given by

$$F_n = (1 + \cos \pi n/M)/2M \qquad n = -M, +M$$

and M is defined as the low pass parameter. This is the same function used in our time window, only here we will be convoluting in the time domain instead of multiplying. The response for this function has been given in the section discussing windows. The first null in this response occurs at a frequency $f = 1/M\Delta t$. We relate the decimation index N to the low pass parameter M by letting $M = 2N + 1$ thus folding the frequency axis just slightly beyond the first null in the filter response. This scheme has been adequate for the types of data which we have encountered, mainly because the power is falling off toward higher frequencies as a result of analog filtering.

The effect of finite record length can also be reduced by filtering. In order to examine one region of the spectrum it is necessary to reduce the power in adjacent regions if it is large. This must be done so that relatively large amounts of power will not be "seen" through the side lobes of the spectral window. In our case, the earth tide with a period of 12.5 hours is the major contribution to low frequency power, and a rather strong high pass filter is required to remove it. The coefficients of a high pass filter can be constructed from a low pass filter in the following manner. Multiply the coefficients by -1, this effectively turns the response upside down; then add 1 to the central coefficient, this adds a constant to the response at all frequencies, and the result is a high pass filter. Carrying this out on the filter described

above we get a high pass filter specified by a new parameter H (in place of M). Where before the period $M\Delta t$ corresponded to the first null in the response, now $H\Delta t$ corresponds to the period at which the response reaches a maximum and starts cutting the low frequencies. We define the nominal pass band as the region between $H\Delta t$ and $M\Delta t$.

Power Spectra and Cross Spectra

The power spectrum, a concept of generalized harmonic analysis is computed by forming the covariance function and taking its cosine transform. This is not always equivalent to squaring the modulus of the Fourier transform. For a discussion of generalized harmonic analysis see Lee (1960, chapter 2).

The covariance function of the sequence (x_i), $i = 1, N$, for p lags corrected for the observed mean is given by Tukey (1959) as

$$C_{xx}(p) = \frac{1}{N-p}\left[\sum_{p}^{N-p} X_i X_{i+p} - \frac{1}{N-p}\left(\sum_{1+p}^{N} X_i\right)\left(\sum_{1}^{N-p} X_i\right)\right]$$

If the covariance is computed for M lags, then the power spectrum can be calculated by the following expression

$$P_{xx}(h) = \frac{1}{M} C_{xx}(0) + \frac{2}{M} \sum_{p=1}^{M} C_{xx}(p) \cos \frac{\pi p h}{M}$$

In an analogous manner, the cross spectrum for two series X and Y can be defined as the complex Fourier transform of the covariance function $C_{xy}(p)$ where p runs from -M to +M lags. A complete statistical treatment of the concept of joint power distributions

has been given by Goodman (1957). For our purposes, since we are dealing with impulsive excitations, it is sufficient to consider the cross spectrum as the power that is common to both series. Given the two series X and Y, the power spectrum for each, P_{xx} and P_{yy}, and the complex cross spectrum P_{xy}, we can define the complex coherence as

$$R_{xy}^2 = \frac{P_{xy}}{(P_{xx}P_{yy})^{1/2}} \qquad 0 \leq |R_{xy}| \leq 1$$

In the analysis of earthquake signals, which are essentially the impulse response of the earth plus random seismic noise, the coherence is a measure of the noise to signal ratio. In this case it is in no way a measure of how closely the two signals resemble each other. If we considered a system which transformed X into Y and added a certain amount of noise in the process, the coherence would be the fraction of power in Y which could be attributed to a linear transformation of X.

Since the operation of forming the covariance in time corresponds in the frequency domain to multiplication of the spectrum of one by the complex conjugate of the other, the argument of the cross spectrum (or the coherence) will be the phase difference between the transforms of the two functions. The more sophisticated view of coherence necessary for random processes is not essential here, we would only say that computing the phase difference by cross spectral analysis tends to reduce the errors due to the already small amount of random noise present on a seismogram.

We use cross spectral analysis when comparing the amplitude

and phase spectrum between two stations, two earthquakes, or two components of motion.

Periodogram Analysis

The periodogram $G_T(f)$ of a function $F(t)$ can be defined as

$$G_T(f) = \frac{1}{T}\left|\int_0^T F(t)e^{-2\pi ift}dt\right|^2$$

Its use to estimate the spectrum of a strictly transient function can be easily justified by choosing T such that the contribution to the integral of the function from T to ∞ is less than some preassigned value. For a periodic function, we need only choose T equal to a multiple of the period to get the formal definition of the line spectrum of a periodic function. When the function is neither transient nor periodic but contains a random continuing component, as does much experimental data, then periodogram analysis can be used only with great caution. Jenkins (1960) states that misuse of the periodogram "has been responsible for the acceptance of probably more false hypotheses than any other statistical or applied mathematical tool."

The earth's free oscillations are essentially damped sinusoidal vibrations, so we consider them as transient and take records long enough for the signal to be essentially zero by the end of the record. In this approach it is necessary to know what proportion of the power is due to continuing seismic noise, as this part will control the variance of the computed spectral estimates. It has been shown by Jenkins (1960) that the periodogram is not a reasonable estimator for the spectrum of

a random function because although the mean value of the spectrum for long samples converges to the proper value, the variance does not become small. This is the reason why Fourier analysis of white noise (random numbers) does not produce a smooth flat spectrum, but a very jagged one. For this reason we have only used periodogram analysis where we feel it is justified by the transient nature of the signal, and we have tried to estimate what the noise level will be in these cases. We have used this method in measuring the amplitude spectra as a function of time, the Q of the earth by the bandwidth, the fine structure of the spectrum requiring high resolution, and absolute phase measurements referred to the origin time of the source.

Noise

In our work with digitized seismograms the noise sources which appear to be important are as follows:

1) Timing errors, non-uniform drum speed
2) Instrument drift
3) Reading errors due to thick traces or tangled traces
4) Paper stretch
5) Base line errors
6) Barometric pressure changes
7) Wind
8) Local earth noises including man-made disturbances
9) Earth tide
10) Tilt of coastal regions due to ocean tide loading.

Errors 2), 5), 9), and 10) can be minimized by high pass filtering unless

they are close to a frequency of interest. For example, using a standard 1 r.p.h. drum seismogram, a slight stretch in the paper can produce a small distortion in the base line. This shows up in the spectrum as a very strong peak at a period of 1 hour. As a result, we do not anticipate much success in measuring the gravest mode of the earth which has a period of 53.5 minutes using this type of seismogram.

Timing errors are reduced by the digitizing technique we employ, dividing the distance between minute marks into proportionate parts.

Errors 6), 7), and 10) can be considered as signals, and independent recording devices could be set up to measure them. Their effect on the measurement of the earth's spectrum could then be corrected for directly in the frequency domain. As a first step we have analyzed ocean tide recordings and found a significant effect on the low frequency spectrum as will be discussed in a later section. Long period recordings of barometric pressure changes are available for the Pasadena station, and an analysis is planned for this data.

The only effective way of treating local earth noises for which the source is not known is by cross spectral analysis of widely separated stations, which allows separation of all signals that are not coherent over large geographical areas. This has been our approach, and it has been remarkably successful for pairs of stations such as Pasadena-Berkeley, Pasadena-Tiefenort, and Isabella-Ñana.

We have estimated the random noise introduced by reading the analog records by repeating the complete analysis of several records using entirely different methods. The agreement between the spectra

computed for these different sets of data representing the same signal was very good, especially at the lower frequencies, and on this basis we estimate that the random errors introduced in digitizing the records are very small compared with other local effects that distort the spectrum.

III. RESULTS OF POWER SPECTRAL ANALYSIS

Notation

In our first paper, and in many of the figures included here we have used the notation of Pekeris (1959) for spheroidal modes and that of Gilbert and MacDonald (1959) for toroidal modes. These notations have not been consistant. Henceforth the following notation proposed by MacDonald and Ness (1961) will be used.

$$ {}_nS_\ell^m \quad \text{and} \quad {}_nT_\ell^m $$

The number of radial nodal surfaces is given by n, the surface harmonic dependence on the polar angle by ℓ, and the azimuthal dependence by m. To convert the notation in our figures, substitute an arabic number for the roman numeral used for n in the spheroidal modes, and subtract 1 from the index n used for the toroidal modes. Note that if n has been left blank it means that $n = 0$, but if m is left blank it means that we are considering the degenerate case where m runs from $-\ell$ to $+\ell$ and the frequency of the mode remains unchanged.

Isabella-$\tilde{\tilde{N}}$ana

Comparison of the spectra for these two strain instruments has been our most successful method for determination of the periods of free oscillations. Figures 2 and 3 show the remarkable similarities between the low frequency seismic spectrum of the Chilean earthquake recorded in Peru and in California. There are a number of questions about the interpretation of thedata shown in these figures. Fine structure

analysis has shown that ${}_0S_2$ is correctly identified, however the period of the ${}_0T_2$ mode is not correct. As will be discussed in a later section, the ${}_0T_2$ mode may be split into one of two possible groups of 5 lines each which means the period of ${}_0T_2^0$ can be either 43. 31 or 42. 94 minutes. MacDonald and Ness (1961) have stated that the identification of ${}_0T_5$ and ${}_1S_3$ is incorrect. They have identified a double peak at 17. 68 and 17. 88 minutes as ${}_1S_3$. The presence of a peak at 17. 88 minutes on an instrument presumably recording only vertical motion certainly questions our identification of 17. 9 min. as a toroidal mode. However our original identification of the peak at 17. 9 minutes as ${}_0T_5$ was based on the large response of the NS and EW horizontal pendulum seismographs at this period and the absence of any response on the vertical component (see fig. 4). Analysis of a longer record from the Isabella strain instrument casts doubt on the interpretation of any peaks in this region recorded at Isabella as can be seen in fig. 3a. In view of this, we will rely on the $\tilde{N}\tilde{a}na$ observation and tentatively identify the peak at 17. 96 minutes as ${}_0T_5$.

The power spectrum calculation on the extended Isabella record used 2000 lags at $\Delta t = 2$ minutes for a total record length of 38, 200 minutes. The radial mode ${}_0S_0$ with a period of 20. 46 minutes is now visible (fig. 3a), and the single peak at 13. 5 minutes has been resolved into three separate peaks. As can be seen in fig. 2, there are three possible modes very close together in this region, ${}_0S_7$, ${}_0T_7$, and ${}_2S_3$. The observed peaks are now at 13. 65, 13. 53, and 13. 35 minutes. The identification of the one at 13. 53 as ${}_0S_7$ (see Table I) is based on the fact that its amplitude is comparable to the adjacent spheroidal modes

${}_0S_5$, ${}_0S_6$, and ${}_0S_8$. The peak at 16.03 minutes shown in fig. 3a is definitely broader than can be attributed to a single line. Unless this is due to the rotational splitting, which will be discussed in a later section, we have no explanation for this broadening.

A revised table of the free oscillation periods measured with the extended Isabella record is given in Table I. The increased frequency resolution permits us to quote these periods to 4 significant figures.

Pasadena-Berkeley

This analysis represents our best separation of vertical motion, however the length of record was too short to resolve the problems of identification of the higher modes. The instruments used were two Press-Ewing 30-90 vertical seismometers, one at Pasadena and one at Berkeley. The cross spectrum is shown in fig. 5. It seems doubtful that ${}_1S_3$ is strongly excited as the only peak between ${}_0S_5$ and ${}_0S_6$ in this analysis is a rather small one at a period of 17.4 minutes. The small peak between ${}_0S_6$ and ${}_0S_7$ at a period of 15.0 minutes is probably ${}_2S_2$. The use of an instrument with a 30 second pendulum to interpret modes with periods down to 20 minutes seems justified by the good agreement with observations made by other instruments. The observation of spheroidal modes from ${}_0S_7$ on adds nothing new to our knowledge of the earth's spectrum, but the phase information for these modes is an indication of the properties of the exciting source as will be discussed later. An interesting point is the absence of the ${}_0S_9$ mode in this cross spectrum.

Tiefenort N-S and E-W

The records for a double pendulum instrument designed for measuring the earth tide were made available to us by Professor W. Buchheim at Freiberg. The station is at Tiefenort, East Germany and has both a N-S and E-W component. The records had to be photographically enlarged by a factor of 10 before they could be digitized at one minute intervals, so there is a relatively large error introduced by the thickness of the trace. The individual power spectra and the cross spectra of these two instruments is shown in fig. 7. From this analysis it is clear to what extent these horizontal instruments are responding to tilt associated with the spheroidal modes. Many of the modes can be identified by comparison with the theoretical values for a Gutenberg model earth which are plotted on the figure. Because of the short record (24 hours) and large expected error as mentioned above, a table of observed periods and identifications will not be presented here as it could not materially add to our knowledge of the periods. One of the more interesting things to result from this analysis is the phase difference between the two horizontal components. For a stationary source, or a moving point source we would expect only a difference of 0 or π in phase. As soon as one postulates a moving dipole source, however, these phases can take on any intermediate value. This effect will be discussed in a later section.

Pasadena-Tiefenort E-W

Cross spectral analysis was performed on the Tiefenort E-W com-

ponent and a long period horizontal E-W instrument at Pasadena and is shown in fig. 6. Both these instruments are responding to tilt as well as horizontal acceleration. Since the response to toroidal motion is good, we have made a tentative identification of toroidal modes from ${}_0T_4$ to ${}_0T_{12}$, and it is given in Table II. It largely confirms our estimates of these modes made from the Isabella and Nana strain. There is, of course no assurance that for some of these, particularly the higher modes, the response is to tilt associated with overtones of spheroidal modes. The best approach to the problem of mode identification depends heavily on the separation of vertical from horizontal motion. This can be accomplished quite well with arrays of 3 component instruments, however in this study the records of pendulum instruments were not sufficiently long to separate components of motion for the higher modes. A further complication enters of course if the toroidal modes couple to produce vertical motion as has been suggested by MacDonald and Ness (1961).

As before, the complex cross spectrum gives us a measure of phase difference between stations as a function of mode number.

TABLE I

REVISED FREE OSCILLATION PERIODS RESULTING FROM ANALYSIS OF A 636 HOUR INTERVAL OF THE ISABELLA STRAIN RECORD

Period in min.	Mode	Period in min.	Mode
53.82	${}_0S_2^0$	11.78	${}_0S_8$
42.94 or 43.31	${}_0T_2^0$	11.00	?
35.55	${}_0S_3^0$	10.57	${}_0S_9$
28.67	${}_0T_3$	10.33	${}_0T_{10}$
25.77	${}_0S_4$	9.668	${}_0S_{10}$
24.49	${}_1S_4$	9.581	${}_0T_{11}$
21.80	${}_0T_4$	8.954	${}_0T_{12}$
20.46	${}_0S_0$	8.934	${}_0S_{11}$
19.80	${}_0S_5$	8.368	${}_0S_{12}$
18.24	?	7.882	${}_0S_{13}$
16.03	${}_0S_6$	7.466	${}_0S_{14}$
15.44	${}_0T_6$	7.095	${}_0S_{15}$
15.07	${}_2S_2$	6.777	${}_0S_{16}$
13.65	${}_0T_7$	6.488	${}_0S_{17}$
13.53	${}_0S_7$	6.226	${}_0S_{18}$
13.35	${}_2S_3$	5.993	${}_0S_{19}$
12.29	${}_0T_8$	5.776	${}_0S_{20}$
12.06	${}_2S_4$		

TABLE II

COMPARISON OF TOROIDAL MODES MEASURED BY CROSS SPECTRAL ANALYSIS OF TWO PAIRS OF HORIZONTAL INSTRUMENTS

Mode	Period in minutes	
	Pasadena Tiefenort	Isabella Nana
${}_0T_4$	21.6	21.80
${}_0T_5$	18.0	17.96
${}_0T_6$	15.3	15.44
${}_0T_7$	13.5	13.65
${}_0T_8$	12.2	12.29
${}_0T_9$	--	11.29
${}_0T_{10}$	10.3	10.33
${}_0T_{11}$	9.68	9.581
${}_0T_{12}$	9.02	8.954

IV. FINE STRUCTURE

Rotational Splitting of the Earth's Free Oscillations

It was noted in the papers by Benioff, Press, and Smith (1961), and by Ness, Harrison and Slichter (1961) that several of the lower spheroidal modes were appearing as doublets or triplets instead of as single lines as would be expected for a stationary elastic sphere. It was suggested by Gilbert and MacDonald (1959) that the spectral lines of the earth would be split by the departure from sphericity and the rotation of the earth. Backus and Gilbert (1961), Pekeris, Alterman, and Jarosch (1961), and MacDonald and Ness (1961) have shown by various perturbation techniques that the additional forces that are present in a rotating system completely remove the degeneracy of an oscillating elastic sphere and split the nth mode of spheroidal or toroidal oscillation into $2n+1$ lines. They have also shown that the oblateness of the earth is a second order term compared to the rotation.

To obtain a frequency resolution sufficient to measure these closely spaced multiplets requires great lengths of record, the length chosen is limited only by dissipation and noise. The only instrument from which we could obtain a long uninterrupted recording of the Chilean earthquake was the Benioff strain seismometer at Isabella, California. The recording was digitized for an interval of 636 hours following the earthquake. With present estimates of the Q for the gravest mode, we would expect its amplitude to be down by less than $1/e^2$ after this length of time. Working with this great length of record has introduced a relatively large amount of noise in proportion to the average level of signal, especially

for the higher modes. By noise we mean extraneous signals, not necessarily random in character. In most of the analyses described in this section, we repeated the calculations for the first half of the record (318 hours) to see the variability in the spectrum caused by such noise. In some cases the variability is great enough to reject the results entirely.

Following Backus and Gilbert (1961), the perturbation in frequency due to rotation of the earth is given by $m\beta_n F$ where m is the azimuthal degree of the surface harmonic, F is the frequency of the earth's rotation, and β_n is the splitting parameter for the nth mode. The $2n+1$ split lines for the nth mode will then have frequencies

$$f_n^m = f_n(1 + m\beta_n/1440) \text{ cycles per minute}$$

where f_n is the degenerate frequency of the nth mode. For spheroidal modes, β_n is a function of the properties of the earth, but for toroidal modes it depends only on the order of the mode. We have measured β_n for three spheroidal modes and for 2 toroidal modes. A comparison of the observed values with the theoretical is given in table III. The amount of confidence placed in these measurements is discussed below.

Since the splitting considered is in the form of a perturbation, it can only provide a measure of how widely spaced the $2n+1$ lines will be, not of their absolute frequency. To make a comparison with a theoretical earth model which does not take into account rotation, we must use the line for $m = 0$. The period for this line of each split mode is given in table III. The uncertainties listed do not take into account the

possible misidentification of a line. Two possible values are listed for ${}_0T_2^0$ as will be explained below.

Spheroidal Mode ${}_0S_2$

Figure 8 shows that 3 out of the possible 5 lines for this mode have been excited. The theoretical values of Backus and Gilbert (1961) are indicated by the arrows at the bottom of the figure. Vertical lines are drawn through the observed peaks which are in very good agreement with the theory. The dashed line indicates the results of analyzing only the first half of the record. There is a marked difference in the relative amplitudes of the 3 split lines for the two lengths of interval that were used. The central line ${}_0S_2^0$ appears to be increasing relative to the other lines. This indicates that the dissipation is much lower for this harmonic, or that energy is being maintained either by additional sources or by coupling from the adjacent lines. A detailed analysis is now under way in which the 636 hour record is divided into many overlapping sections and each section is analyzed separately. This will show more clearly the time dependence of energy in these 3 lines. If the changes are abrupt it will indicate that perhaps additional sources have acted during the 26 day interval.

The period of the central line is 53.83 ± 0.04 minutes. We place a great deal of confidence in the identification of this mode and the determination of its period. The Q measured from width at half power is 350, however if energy is being transferred to this mode, this value will not be a measure of dissipation.

Spheroidal Mode $_0S_3$

Figure 9 shows that 5 out of the possible 7 lines have been excited. In this figure only the theoretically predicted lines are drawn, as they are as close a fit to the observed peaks as could be determined. Again, as in the $_0S_2^0$ mode, the central line $_0S_3^0$ is increasing relative to the adjacent lines.

The period of the central line is 35.55 $\pm$ 0.02 minutes and there is little doubt that the identification is correct.

Spheroidal Mode $_0S_4$

Figure 10 shows a possible interpretation of this mode as 9 equally spaced lines. A theoretical value for the splitting is not yet available. If this interpretation is correct, and there is some doubt that it is, then the period of the central line is 25.89 minutes, and the splitting parameter is 0.14.

Toroidal Mode $_0T_2$

Figure 11 shows two possible interpretations of the 5 way split expected for this mode. In the previous analysis, $_0T_2$ was thought to have a period of 42.3 minutes from a rather broad peak in the power spectrum. With a longer record and a finer resolution it now appears to be considerably lower in frequency. One possible interpretation is indicated by the vertical lines drawn through 5 peaks. If this is correct then the period of the central line is 43.31 $\pm$ 0.10, the splitting parameter is 0.26 and Q is about 400 from the bandwidth of $_0T_2^{-2}$. Both the splitting

parameter and Q are much larger than would be expected for this mode. The other possible interpretation is shown by the small lines near the bottom of the figure. If one assumes that the peaks at 43.97 and 43.63 minutes are spurious, then it appears that the two pairs ${}_0T_2^{-2}$ ${}_0T_2^{-1}$, and ${}_0T_2^{1}$ ${}_0T_2^{2}$ are unresolved, the splitting parameter is about 0.16, and the Q approximately 160. This much more reasonable interpretation which gives a period for the central line of 42.94 minutes depends on being able to reject the two extraneous peaks mentioned above, and at this point there is no justification for doing this. Further analysis to examine the behavior of these peaks as a function of time may provide such a criteria.

Toroidal Mode ${}_0T_3$

Figure 12 shows 7 equally spaced lines, which is our interpretation of this mode. The difference between the analysis of the short and long record is not too great for the peaks indicated by the vertical lines. This is not true for the large peaks on either side of the 7 lines that we have indicated, and on this basis they were discarded as being spurious. If the interpretation is correct, the period of the central line is 28.51 ± 0.05 minutes, and the splitting parameter is 0.14. The splitting is again considerably larger than the theoretical value of 0.083. If this is the true spectrum of the ${}_0T_3$ mode, then the Q must be about 400, which is considerably larger than evidence for other shear type motions would indicate (Sato, 1958). This fact in itself casts doubt on the observation of the split ${}_0T_3$ mode.

Radial Mode $_0S_0$

Figure 13 shows a single peak at 20.458 $\pm$ 0.006 minutes. This mode is nondegenerate and is therefore not split. The Q from bandwidth is about 900.

These observations of the fine structure of the earth's spectrum are considered as preliminary results. Much of the uncertainty is due to the fact that we have available only one example of a source that excited the free oscillations. Another sample with which to work would perhaps resolve some of the problems outlined above. Further analyses as described in the discussion of the $_0S_2$ and $_0T_2$ modes may clarify a few specific points.

TABLE III

RESULTS OF FINE STRUCTURE ANALYSIS COMPARED WITH ROTATIONAL SPLITTING

Mode	Period of central line in minutes	Observed splitting parameter	Theoretical splitting parameter
${}_0S_2$	53.82 ± 0.04	0.41	0.3984
${}_0S_3$	35.55 ± 0.02	0.18	0.1845
${}_0S_4$	25.89 ± 0.03	0.14	---
${}_0T_2$	43.31 ± 0.10 or 42.94 ± 0.10	0.26 or 0.16	0.1667
${}_0T_3$	28.51 ± 0.05	0.14	0.0833

V. SOURCE PROPERTIES

General Considerations

In principle, an observation of the amplitude and phase of all the modes of the earth will permit a complete specification of the initial state of the system, that is the displacements and velocities at time zero when the source acted. Even the observation of a finite number of modes, say all those with frequencies less than some fixed frequency, would permit a partial synthesis of at least the low surface harmonic dependence of the source. Unfortunately, the observations are not good enough at this point to undertake even a limited synthesis of the source. However, by applying some of the information already known about earthquake sources, in the form of certain assumptions about the mathematical representation of a fault, the free oscillation data can be made to yield some new insights into the dynamics of faulting.

For a point source the vector components of displacement for each mode should have an initial phase of 0 or π depending on the value of the surface harmonics at the point of observation. This is easily seen by considering a standing wave in one dimension. The time variation at each point has a phase of 0 or π with respect to the point at which the source acted. When the source is distributed in space however, the one-dimensional analogy is no longer valid, and initial phases of the components of displacement other than 0 or π are possible.

It was noted early in this study that the experimentally determined initial phases for vertical and horizontal displacements could not be 0 or π for all frequencies because the measured phase differences between

these components varied continuously and approached $\pi/2$ for the higher spheroidal modes. Since the spheroidal modes can be considered as a standing wave interference pattern of Rayleigh waves propagating in opposite directions around the earth, and each propagating wave has a phase shift of $\pi/2$ between vertical and horizontal components, the observed shift for spheroidal modes was interpreted as due to preferential radiation of Rayleigh waves in one direction. The amount of this preferential radiation as a function of mode number is a measure of certain dynamic properties of the source. If the sequence of aftershocks outlines the direction and extent of faulting, and it is assumed that the faulting proceeds continuously along this direction at some finite rupture velocity, then the phase shift measurement outlined above will allow a rough determination of the rupture velocity. A description of the method for modeling a fault by a moving point source of normal stress has been given by Benioff, Press, and Smith (1961), and their result for the Chilean earthquake indicated a rupture velocity of between 3 and 4 km/sec and a fault length of about 1000 km.

This method has been generalized to include a moving dipole source which gives rise to phase shifts between the three vector components of displacement on a sphere. The extension to phase shifts between horizontal components allows us to use the lowest modes recorded on strain instruments and tiltmeters previously not permitting interpretation due to the absence of a vertical component. However, as will be pointed out, the present data is such that consideration of a dipole source rather than a vertical force has not materially added to our knowledge of the dynamic properties of the Chilean earthquake. The important result is that the

aftershocks do outline the extent of faulting, and the rupture does propagate at a velocity near that of Rayleigh waves.

An alternate interpretation of the effect of a moving source in terms of the degenerate modes of a sphere will be presented. This interpretation is useful because in the case of the real earth, the degeneracy is removed by rotation, and this method permits the calculation of the amplitudes and phases of each split line as a function of the dynamic properties of the source.

Theory of a Travelling Disturbance

The motion of an elastic sphere can be separated into spheroidal and toroidal types. The spheroidal motion which corresponds to Rayleigh waves is characterized by vanishing radial component of curl. The toroidal motion which corresponds to SH waves has non-zero curl only in the radial direction. These two types of motion may be expressed in terms of the vector spherical harmonics $\underline{P}$, $\underline{B}$, and $\underline{C}$ defined by Morse and Feshbach (1953).

$$\underline{u}^T = \sum_{\ell=1}^{\infty} \sum_{m=0}^{\ell} Z(r)\underline{C}_{m\ell}(\theta, \varphi)\exp(i\omega^T_{m\ell}t) \qquad (1)$$

$$\underline{u}^S = \sum_{\ell=1}^{\infty} \sum_{m=1}^{\infty} (X(r)\underline{P}_{m\ell}(\theta, \varphi) + Y(r)\underline{B}_{m\ell}(\theta, \varphi))\exp(-i\omega^S_{m\ell}t) \qquad (2)$$

The functions X, Y, and Z depend on the distribution of elastic parameters with depth, $\omega^T_{m\ell}$ and $\omega^S_{m\ell}$ are the angular frequencies of the modes T^m_ℓ and S^m_ℓ respectively. From these series we will extract one term

to use as the response of an elastic sphere to an elementary source.

In the subsequent development we will superpose elementary sources lagged in time and space to get the equivalent of a moving source. The choice of the elementary source comes from the observation of the first motion patterns for P and S waves. The P wave first motion pattern for most earthquakes associated with faulting shows a quadrant distribution about the fault direction, that is the sign of the motion changes as the observation point passes from one quadrant to the next, and the maximum amplitude occurs near angles of $\pi/4$, $3\pi/4$ and so forth. If this observed amplitude distribution were expanded in terms of surface harmonics $P_n^m(\cos\theta)\sin m\varphi$, the largest term in the series would be that for $m = 2$. We expect the same distribution for Rayleigh waves. For SH waves, the first motion pattern indicates that the surface harmonic $P_n^1(\cos\theta)\sin\varphi$ is the predominate one. Thus from the series representation of the displacements of an elastic sphere given in equations 1 and 2, we take the term that has a $\sin 2\varphi$ dependence for spheroidal motion and a $\sin\varphi$ independence for toroidal motion and use these terms to represent the response of the earth to an elementary source which is physically similar to an observed earthquake.

The expressions for the components of displacement for spheroidal modes due to an elementary source located at the pole of the spherical coordinate system and acting at time zero are as follows:

$$u_r = U(r)P_n^2(\cos\theta)\sin 2\varphi \tag{3}$$

$$u_\theta = -\frac{V(r)}{\sin^2\theta}\left[\, n\cos\theta\, P_n^2(\cos\theta) - (n+2)P_{n-1}^2(\cos\theta)\right]\sin 2\varphi \tag{4}$$

$$u_{\varphi} = - \frac{2V(r)}{\sin \theta} [P_n^2(\cos \theta)\cos 2\varphi] \qquad (5)$$

where U and V are functions that depend on the mode number and the variation of elastic parameters with depth. A parallel development for the toroidal modes can be carried out, however the observations of these modes have not been good enough to justify such a calculation here.

If this source is now displaced an amount x along a fault which makes an angle φ with the great circle path to the receiving station, the coordinates of that station with respect to the new position of the source are θ' and φ' where

$$\cos \theta' = \cos (x/R)\cos \varphi + \sin \theta \sin \varphi \sin (x/R)$$

R is the radius of the earth, and

$$\sin \varphi' = (\sin \theta \sin \varphi)/\sin \theta'$$

The source will not arrive at this point x until a time τ after the origin time, and this time τ will be equal to x/v where v is the average velocity with which the source has moved during the time it took to traverse the distance from 0 to x. Furthermore, the amplitude of the source at this later time may be less, and the average velocity of rupture may have changed as will be discussed later, so we multiply by some amplitude function A(x), and consider the velocity to be a function of x, v(x). The vector components of the infinitesimal contribution to vibration of the nth spheroidal mode by such a source can be integrated over the length of the fault L, which has been chosen to be in the direction of the azimuth $\varphi = 0$. The displacements are given by

$$u_r = U(r)\int_0^L A(x)P_n^2(\cos\theta(x))\sin 2\varphi(x)\exp(-i\omega_n\tau(x))\,dx \qquad (6)$$

$$u_\theta = V(r)\int_0^L A(x)[(n+2)P_{n-1}^2(\cos\theta(x)) - n\cos\theta(x)P_n^2(\cos\theta(x)]$$

$$\times\left[\frac{\sin 2\varphi(x)\exp(-i\omega_n\tau(x))}{\sin^2\theta(x)}\right]dx \qquad (7)$$

$$u_\varphi = V(r)\int_0^L \frac{A(x)}{\sin\theta(x)}[P_n^2(\cos\theta(x))\cos 2\varphi(x)\exp(-i\omega_n\tau(x))]\,dx \qquad (8)$$

The decay law A(x) for the source has been included because the intensity of radiation from a moving crack should decrease with distance due to the fact that it is continuously releasing stress as it moves along which decreases both the intensity of the strain field and the volume over which it is being released. Since the intensity of the strain field is decreasing, it was originally thought that the velocity of rupture might change also, so it is included as a function of x. We now feel that the concept of a moving dipole or vertical force as a representation of a real fault is sufficiently crude that such refinements in the concept of a fault velocity other than as an average velocity may be meaningless.

For fault lengths small compared with the circumference of the earth, and for velocities such that the time of propagation is small compared with the period of the mode considered, the integrands in equations 6, 7, and 8 are slowly oscillating functions over the range of integration, and numerical integration is justified. In fact it is preferable to use a finite sum rather than an approximation of the integrand that would permit exact evaluation of the integral because we may wish to simulate the

earthquake by a small number of individual fractures instead of one long continuous rupture.

These three complex integrals have been programmed for an IBM 7090 computer. The six integrands, real and imaginary parts of the three components for different fault lengths and rupture velocities are carried as a three-dimensional array $S_{i,j,k}$ where i is the mode number, j is the fault length, and k is the component of displacement. With this arrangement it is possible to carry out the six integrations simultaneously, and use different fault lengths without having to repeat any parts of the integration. In addition to the three phase differences this program computes the absolute phase lag of each component referred to the origin time of the source ($\pm 2n\pi$), and the ratio of amplitude of the two horizontal components. This last quantity is only capable of calculation due to the fact that both horizontal components have the same functional dependence on r, namely $V(r)$.

The amplitude and velocity functions are defined in the program as Fortran FUNCTION subprograms and thus may be changed to any desired function without altering the rest of the program. Each of these functions is made to depend on a parameter which is read in at the start of each run. For a given functional relationship, the parameter determines how rapidly the amplitude or velocity change with distance. If the parameters are zero, the functional relation reduces to a constant. For example, in the preliminary work on this problem the amplitude function has been defined as $e^{-\alpha x}$ where α is the parameter and x the distance.

Since the initial phases of the three components of motion at each station are computed directly, we can consider pairs of stations and evaluate the phase difference for one component of motion at two stations. Neither the phase shift between the two horizontal components at one station, or the phase for one component at two stations is easy to observe experimentally. The reason is that by horizontal components we do not mean NS and EW, but θ and φ referred to a coordinate system with its pole at the epicenter. The practical separation of these components has not been possible in the data we have analyzed. For some stations one can say that a particular geographical component is responding mostly to θ or φ motion, for example Isabella which is oriented N 32° W is almost along a line drawn from the epicenter, so it can be considered to be measuring θ motion only. The results that will be shown here reflect this poor separation of coordinates.

Comparison of Theory With Observations

In all the results that follow, experimentally determined phase shifts were obtained by cross spectral analyses of records covering the same interval of time. In most cases the individual time corrections at stations provided a phase correction smaller than the other uncertainties involved in the measurement of phase.

Figure 14 shows the phase difference for the θ component of motion at Isabella and Nana. The solid line represents the theoretical values for a fault of length 1000 km with a rupture velocity of 3 km/sec. The open circles are the observed phase differences between the NW

components of strain at the two stations. Repetition of this calculation for other fault parameters showed it to change only slightly. A change in station coordinates which is equivalent to a change in the assumed azimuth of the fault (since this determines the coordinate system used) produces a radical change in the pattern so this calculation, although it is not sensitive to length and velocity may aid in the determination of the fault azimuth.

Figure 15 shows the phase difference between θ and φ components for the Nana station computed for a 1000 km fault and a rupture velocity of 3 km/sec. The measured phase between the components which are oriented NW and NE is shown by the open circles. The fit is poor, and no improvement is expected for this type of observation without better separation of components.

Figure 16 represents the same situation for the Tiefenort earth tide installation. Here the θ direction makes an angle of 45° with the NS component.

Figure 17 compares the phase between r and θ components for the Berkeley station and several choices of fault parameters. It should be noted that this particular theoretical calculation is independent of the type of elementary source used, giving the same results for a dipole as a point vertical force. This is what would be expected, since the phase shift between components for a propagating Rayleigh wave is independent of the source.

Figure 18 shows the phase difference between vertical components at Pasadena and Berkeley. It is interesting to note that Berkeley leads

Pasadena as would be expected for a fault that propagated from north to south. Also, the pattern indicates that the odd and even modes are behaving differently; this is caused by the particular geographical location of the two stations. An entirely different pattern could be constructed by considering the phase to be continually increasing or decreasing, and adding $2n\pi$ to the observations, however for recognition and comparison with theory, it seems more reasonable to restrict the phases to the range $0, 2\pi$.

Figure 19 shows the effect of a decaying source on the pattern for r, θ phase shift at the Pasadena station. The solid line is the constant amplitude source and the dashed line is for a source that has decayed to $1/e$ of its original amplitude at a distance of 500 km. The pattern is stretched out toward the higher frequencies. If the observations were more precise, and the model more realistic, the effect of a decaying source would be important. In view of the degree of approximation considered this effect does not change the main result obtained by Benioff, Press, and Smith (1961).

Source Characteristics in Terms of the Nondegenerate Modes

The phase relations that have been discussed previously hold for for a moving source on a stationary elastic sphere. They also hold for experimental observations on a rotating sphere provided the frequency resolution is not sufficient to resolve the split lines. If the split lines are resolved, a new theory is needed.

The free modes have been considered as a superposition of waves

travelling about a sphere in opposite directions with those in one direction being enhanced by the directional properties of the source. For an alternate view, consider the independent excitation of the $2n+1$ degenerate eigenfunctions for a given mode. Clearly, the phase measurement we have been considering must be a weighted average of the individual phases of these $2n+1$ lines. In order to measure relative excitation of these degenerate modes, observations at $2n+1$ stations would be necessary. When the degeneracy is removed by rotation and the lines are split, within the limits imposed by dissipation and noise it is possible to measure the individual amplitude and phase of each split line from an observation at a single station.

As before we can write the expressions for the components of displacement on an elastic sphere (equation 2). If we treat the effect of rotation as a perturbation on the frequencies only, and use a coordinate system with a polar axis that corresponds to the axis of rotation of the earth, the vertical displacement for a point source at the pole will be

$$u_\ell = P_\ell^0(\cos\theta)\exp(i\omega_\ell^0 t) \tag{9}$$

Use of the addition theorem for surface harmonics gives the displacement for a point source located at $\theta(x)$, $\varphi(x)$ to be

$$u_\ell = \sum_{m=-\ell}^{+\ell} \frac{(\ell-m)!}{(\ell+m)!} P_\ell^m(\cos\theta) P_\ell^m(\cos\theta(x))\exp[\,im(\varphi-\varphi(x))+i\omega_\ell^m t] \tag{10}$$

Note that the frequency is different for each term of the series. If the source starts at the point $x = 0$ and moves along a line that makes an angle α with the meridian arriving at the point $\theta(x)$, $\varphi(x)$ at a time $\tau(x)$,

we can integrate each term of the sum over x along this direction and compute the relative excitation of the $2n+1$ lines for a moving source. For vertical motion of the mode ${}_0S_\ell^m$ the relative amplitude and phase are given by the complex number u_ℓ^m where

$$u_\ell^m = P_\ell^m(\cos\theta)e^{im\varphi}\frac{(\ell-m)!}{(\ell+m)!}\int_0^L P_\ell^m(\cos\theta(x))\exp(im\varphi(x)-\omega_\ell^m\tau(x))\,dx \tag{11}$$

Since $P_\ell^{-m}(x) = (-1)^m\frac{(\ell-m)!}{(\ell+m)!}P_\ell^m(x)$, the modulus of each term in equation 10 is unchanged by replacing m by $-m$. Therefore the pattern of amplitudes for a multiplet excited by a point source is symmetric with respect to the line $m = 0$. Asymmetry will be introduced by the integration indicated in equation 11 which gives the effect of a moving source. We note that there is little asymmetry in the observed multiplets for ${}_0S_2$ and ${}_0S_3$ shown in figs. 8 and 9. This indicates that compared to the wavelength and period for each of these modes, the fault length and duration of rupture were small.

This asymmetry may be an important factor in the accurate determination of the periods of the higher modes in which the individual split lines are not resolved. In this case the observed maximum in the spectrum will be displaced slightly from the line $m = 0$.

The present data for the amplitudes of the split lines has not been considered accurate enough to justify carrying out the integration of equation 11. Future measurements of great earthquakes recorded automatically in digital form on improved instruments may provide data

with sufficient precision to utilize the method outlined above for determining large scale source properties. The limitation on resolution imposed by dissipation in the earth will however prevent a detailed specification of the source.

VI. EXCITATION BY OTHER GEOPHYSICAL PHENOMENA

Energy Considerations

The energy density associated with a physical phenomenon can be used as a rough criterion to estimate the likelihood that it will excite the free vibrations of the earth to a measurable extent. The distribution of energy with frequency, not the total energy will determine what modes will be excited. MacDonald and Ness (1961) estimate that the energy density for the ${}_0T_2$ mode excited by the Chilean earthquake is 10^{18} ergs/cph, but the total energy release is perhaps 10^{24} ergs. Observations of seismic waves indicate that this energy is distributed over a broad band of frequencies, approximately 0.0003 cps to 10 cps. A source mechanism that involves a smaller total energy but which is restricted to a narrower band of frequencies may be as effective as a great earthquake in exciting certain modes of the earth.

If we use the level of excitation produced by the Chilean earthquake as the minimum level for positive detection of the lower modes, then only those sources with energy densities at least as great as 10^{18} ergs/cph can be considered. The energy density computed for the ${}_0T_2$ mode has been used as an order of magnitude estimate for the energy of the lower spheroidal modes. The only justification for this use is the observed fact that at higher frequencies the energy of Love waves and Rayleigh waves is comparable.

Geomagnetic Events

Benioff* hypothesized that the widespread magnetic field change associated with a magnetic storm might be sufficiently coupled to strain energy by the conducting mantle to excite the lower modes of the earth. Certainly geomagnetic field changes apply a stress to the conducting earth, the earth being elastic does respond, and since any elastic motion can be considered as a superposition of free oscillations, the only question concerns the magnitude of the effect. From the energy viewpoint it appears that this coupling can be measured.

Chapman and Bartels (1940) estimate the energy change associated with the first phase and the main phase of a magnetic storm as approximately 10^{22} ergs each. The energy of the main phase is mostly in the surface harmonic $P_1(\cos\theta)$ with smaller amounts in $P_2(\cos\theta)$ and $P_4(\cos\theta)$ (with respect to the magnetic axis). The energy of the first phase is distributed somewhat more among the higher harmonics. In order to estimate the energy density as a function of frequency we have to relate these harmonics to the natural frequencies of the earth. If the time variation of the field is a step function, then the space dependence mentioned above should restrict excitation to those modes ${}_nS_\ell$ with surface harmonic dependence $\ell \leq 5$. To estimate the radial overtones that would be excited we note that the applied stress will decrease exponentially with depth due to the shielding effect of the outer layers. From this, we would not expect higher order overtones, with radial nodal surfaces at

*H. Benioff, personal communication, 1961.

relatively shallow depths to be excited. Thus the nature of the distributed source leads us to estimate $_2S_5$ with a frequency of 10 cph as a reasonable upper limit for the modes excited by a magnetic storm.

Using this estimate, which is very rough, the energy density will be about 10^{21} ergs/cph. Thus if only 1 part in 1000 of the electromagnetic energy is converted to strain energy, the energy density will still be 10^{18} ergs/cph which we have chosen as the lower limit for detectability.

To test this hypothesis we analyzed the Isabella strain records for two magnetically disturbed periods. Figure 20 is the power spectrum of the interval which includes the great solar flare and associated magnetic storm of Nov. 12, 1960. In this figure it appears that some of the modes are excited, in particular S_4, S_0 or S_5, and $_2S_2$. The mean square power in the region near a period of 1 hour corresponds to about 1/50 of the power measured for the S_2 mode excited by the Chilean earthquake. Thus these peaks are right at the noise level and without a better specification of the noise, we cannot test their significance.

An analysis of the week of July 15-19, 1959 which included two magnetic storms is shown in fig. 21 along with the spectrum of the interval July 19-24, 1959. Although none of the resonant frequencies of the earth appear to be present, there is an increase in the energy level for the magnetically disturbed period that may be significant. Again, the actual values of power are right at the level of background noise, and we do not yet know how much variation in the power level can be expected from one week to the next due to local weather and related effects.

The results of this preliminary work indicates that there may be a

measureable coupling of magnetic energy to strain energy, but the strain energy is no greater than about 5×10^{16} ergs/cph for the lowest modes. In order to make a statistical test of this effect, many more samples of low frequency seismic noise would be needed.

Coupling of Sea Level Oscillations

The frequency range between the ${}_0S_2$ mode and the earth tide shows a number of peaks, some of which are common to more than one station as can be seen in fig. 2. Since the semi-diurnal ocean tide is responsible for an appreciable effect on strain instruments and tiltmeters located within several hundred kilometers of a sea coast, it was suspected that some of the unidentified low frequency peaks might be due to oscillations in the sea level excited by the seismic sea wave.

A cross spectral analysis was performed on a horizontal EW pendulum at Pasadena and the Los Angeles outer harbor tide gage recording for a 24 hour interval starting at the arrival of the seismic sea wave. The seismometer, which has been described by Gilman (1960), is very sensitive to long period tilts. The result of this analysis is shown in fig. 22. The peak at 150 minutes has a coherence of 0.75 and a phase difference of 0.0 radians between tilt down to the west and sea level up. Analysis of a 5 day interval of the tide gage recording showed a pronounced peak at 75 minutes. The rms amplitude of each of these peaks at 75 min and 150 min is about 2 cm.

The conclusion from this work is that no interpretation of periods longer than 1 hour observed on horizontal instruments should be made without measuring and correcting for the tilting effect of nearby sea level

fluctuations. Thus it is not possible with the present data to test hypotheses such as those of Slichter (1961), Gilbert*, or Alterman Jarosch and Pekeris (1959) which involve periods of the core-mantle system which are longer than 1 hour.

*J. F. Gilbert, personal communication, 1961.

REFERENCES

Alsop, L., G. Sutton, and M. Ewing, "Free oscillations of the earth observed on strain and pendulum seismographs," J. Geophys. Res., 66, 631-641, 1961.

Alterman, Z., H. Jarosch, and C. L. Pekeris, "Oscillations of the earth," Proc. Roy. Soc. London A, 252, 80-95, 1959.

Backus, G., and J. F. Gilbert, "The rotational splitting of the free oscillations of the earth," Proc. Nat. Acad. Sci., 47, 362-371, 1961.

Benioff, H., B. Gutenberg, and C. F. Richter, Progress report, Seismological Laboratory, Trans. Am. Geophys. Union, 35, 979, 987, 1954.

Benioff, H., J. Harrison, L. La Coste, W. H. Munk, and L. Slichter, "Searching for the earth's free oscillations," J. Geophys. Res., 64, 1334-1337, 1959.

Benioff, H., F. Press, and S. Smith, "Excitation of the free oscillations of the earth by earthquakes," J. Geophys. Res., 66, 605-619, 1961.

Blackman, R. B., and J. W. Tukey, "The measurement of power spectra," Dover, New York, 1958.

Bogert, B. P., "An observation of free oscillations of the earth," J. Geophys. Res., 66, 643-648, 1961.

Buchheim, W., and S. Smith, "The earth's free oscillations observed on a two component tiltmeter at Tiefenort, East Germany," (to be published), 1961.

Chapman, S., and J. Bartels, "Geomagnetism, Vol. II," Oxford University Press, London, 1940.

Dolph, C. L., "A current distribution for broadside arrays which optimizes the relationship between beam width and side-lobe level," Proc. I. R. E., 34, 335-348, 1946.

Gilbert, J. F., and G. J. F. MacDonald, "Free oscillations of the earth, I. Toroidal oscillations," J. Geophys. Res., 65, 675-693, 1960.

Gilman, R., "Report on some experimental long period seismographs," Bull. Seism. Soc. Am., 50, 553-560, 1960.

Goodman, N. R., "On the joint estimation of the spectra, cospectrum, and quadrature spectrum of a two-dimensional stationary gaussian process, N. Y. U. Eng. Stat. Lab. Scientific Paper No. 10, 1957.

Jenkins, G. M., "General considerations in the estimation of spectra," Stanford Univ. App. Math. and Stat. Lab. Tech. Report No. 4, 1960.

Lamb, H., "On the vibration of an elastic sphere," Proc. London Math. Soc., 13, 189-212, 1882.

Lee, Y. W., "Statistical theory of communications," John Wiley and Sons, Inc., New York, 1960.

MacDonald, G. J. F., and N. F. Ness, "A study of the free oscillations of the earth," (to be published), 1961.

Morse, P. M., and H. Feshbach, "Methods of theoretical physics," McGraw Hill Book Co., New York, 1953.

Ness, N. F., J. C. Harrison, and L. B. Slichter, "Observations of the free oscillations of the earth," J. Geophys. Res., 66, 621-629, 1961.

Parzen, E., "Mathematical considerations in the estimations of spectra," Stanford Univ. App. Math. and Stat. Lab. Tech. Report No. 4, 1960.

Pekeris, C. L., Z. Alterman, and H. Jarosch, "Comparison of theoretical with observed values of the periods of free oscillations of the earth," Proc. Nat. Acad. Sci., 47, 91-98, 1961.

Pekeris, C. L., Z. Alterman, and H. Jarosch, "Terrestrial spectroscopy," Nature, 189, (in press).

Press, F., "Observations of the free vibrations of the earth, (abstract)," J. Geophys. Res., 65, 2518, 1960.

Sato, Y., "Attenuation, dispersion, and the wave guide of the G wave," Bull. Seism. Soc. Am., 48, 231-251, 1958.

Slichter, L. B., "The fundamental mode of the earth's inner core," Proc. Nat. Acad. Sci., 47, 186-190, 1961.

Tukey, J W., "Equalization and pulse shaping techniques applied to the determination of initial sense of Rayleigh waves," Report of the Panel on Seismic Improvement, U. S. Department of State, 1959.

LIST OF CAPTIONS

Fig. 1. Time window and corresponding spectral window used for fine resolution Fourier analysis.

Fig. 2. Power spectra and coherence for Isabella, California and Ñaña, Peru, computed with 500 lags, Δt = 3 minutes, record length = 6932 minutes. Theoretical values for the periods of free oscillations are based on a Gutenberg model earth. Filter notation described by Benioff, Press and Smith (1961).

Fig. 3. Same as fig. 2, for the higher modes.

Fig. 3a. Power spectrum of Isabella, lowpass filter cut off at 0.250 cpm, 2000 lags, Δt = 2 minutes, record length = 38, 200 minutes.

Fig. 4. Power spectra of three component pendulum seismographs at Pasadena, and Isabella strain. Higher modes only are shown, theoretical values are for a Gutenberg model earth.

Fig. 5. Pasadena-Berkeley, cross spectrum of vertical components, low pass filter cut off at 0.60 cpm, 500 lags, Δt = 0.833 minutes, record length = 740 minutes. A linear trend has been removed.

Fig. 6. Pasadena-Tiefenort, cross spectrum of EW components. Nominal pass band, 0.016-0.167 cpm, 200 lags, Δt = 3 minutes, record length = 1155 minutes. A linear trend has been removed.

Fig. 7. Tiefenort, East Germany, power spectra and cross spectrum of NS and EW components. Nominal pass band, 0.012-0.250 cpm, 300 lags, Δt = 2 minutes, record length = 1116 minutes.

Fig. 8. Isabella strain, fine structure of spheroidal mode ${}_0S_2$. Nominal pass band, 0.0125-0.2500 cpm. Fourier analysis of two lengths of record, 19,100 and 38, 200 minutes, Δt = 2 minutes. Calculated rotational splitting indicated at the bottom of the figure.

Fig. 9. Isabella strain, fine structure of spheroidal mode ${}_0S_3$. Nominal pass band, 0.0125-0.2500 cpm, Fourier analysis of two lengths of record, 19,100 and 38, 200 minutes, Δt = 2 minutes. Calculated rotational splitting indicated at bottom of figure.

Fig. 10. Isabella strain, fine structure of spheroidal mode ${}_0S_4$. Nominal pass band, 0.0125-0.2500 cpm, Fourier analysis of two lengths of record, 19,100 and 38, 200 minutes, Δt = 2 minutes. Observed splitting only is indicated, no theoretical values are available for this mode.

Fig. 11. Isabella strain, fine structure of toroidal mode ${}_0T_2$. Nominal pass band 0.0125-0.2500 cpm. Fourier analysis of one length of record, 19,200 minutes, Δt = 2 minutes. Calculated rotational splitting indicated by short vertical lines at bottom of figure, observed splitting shown by vertical lines through spectral peaks.

Fig. 12. Isabella strain, fine structure of toroidal mode ${}_0T_3$. Nominal pass band 0.0125-0.2500 cpm. Fourier analysis of two lengths of record, 19,100 and 38,200 minutes, Δt = 2 minutes. Observed splitting only is indicated.

Fig. 13. Isabella strain, fine structure of radial mode ${}_0S_0$. Nominal pass band 0.0125-0.2500 cpm. Fourier analysis of one length of record, 38,200 minutes, Δt = 2 minutes. No splitting observed.

Fig. 14. Isabella-$\tilde{N}\tilde{a}na$, observed phase shift between NW components at each station for spheroidal modes. Theoretical phase shift calculated for moving couple source with velocity 3 km/sec and length 1000 km.

Fig. 15. $\tilde{N}\tilde{a}na$, Peru, observed phase shift between NW and NE components. Theoretical phase shift between θ and φ components for a moving couple source with velocity 3 km/sec and length 1000 km.

Fig. 16. Tiefenort, East Germany, observed phase shift between NS and EW components. Theoretical phase shift between θ and φ components for a moving couple with velocity 3 km/sec and and length 1000 km.

Fig. 17. Berkeley, observed phase shift between UD and EW components. Theoretical phase shift between r and θ components for a moving couple or vertical force with velocities of 3 and 4 km/sec and a length of 1000 km.

Fig. 18. Berkeley-Pasadena, observed phase shift between vertical components. Theoretical phase shift between vertical components at these two stations computed for a moving couple or vertical force with a velocity of 3 km/sec and a length of 1000 km. Open circles are for odd order modes, and closed circles for the even order modes.

Fig. 19. Pasadena, theoretical phase shift between r and θ components for a moving source with constant amplitude (solid line) and one the amplitude of which is decaying exponentially with distance (dashed line). Both calculations are for a velocity of 3 km/sec and a length of 1000 km.

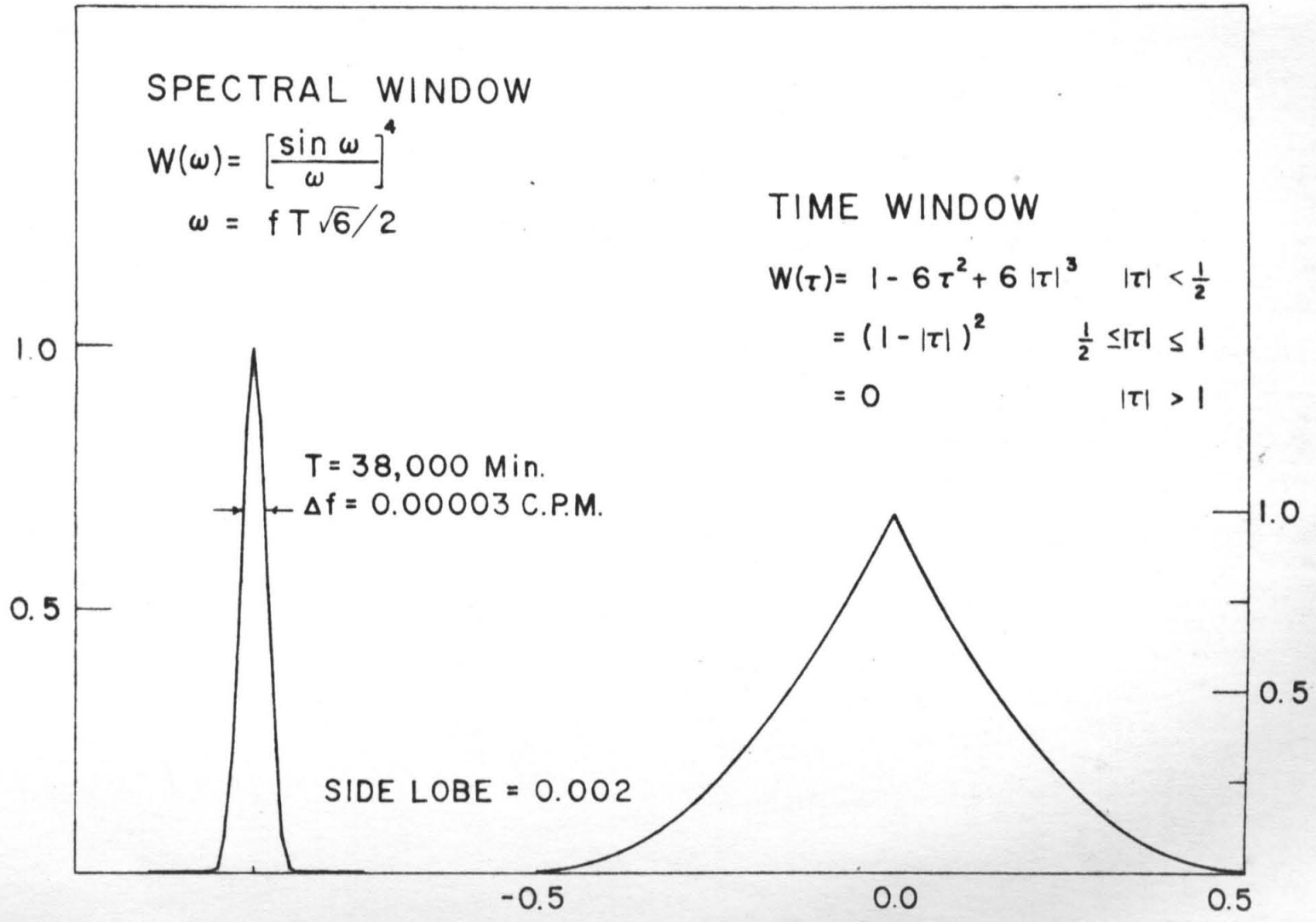
SPECTRAL WINDOW
W(ω)= [sin ω / ω]^4
ω = f T √6/2
TIME WINDOW
W(τ)= 1 - 6τ² + 6 |τ|³ |τ| < 1/2
= (1 - |τ|)² 1/2 ≤ |τ| ≤ 1
= 0 |τ| > 1
1.0
0.5
T = 38,000 Min.
Δf = 0.00003 C.P.M.
SIDE LOBE = 0.002
-0.5
0.0
0.5
1.0
0.5

FIG. 1

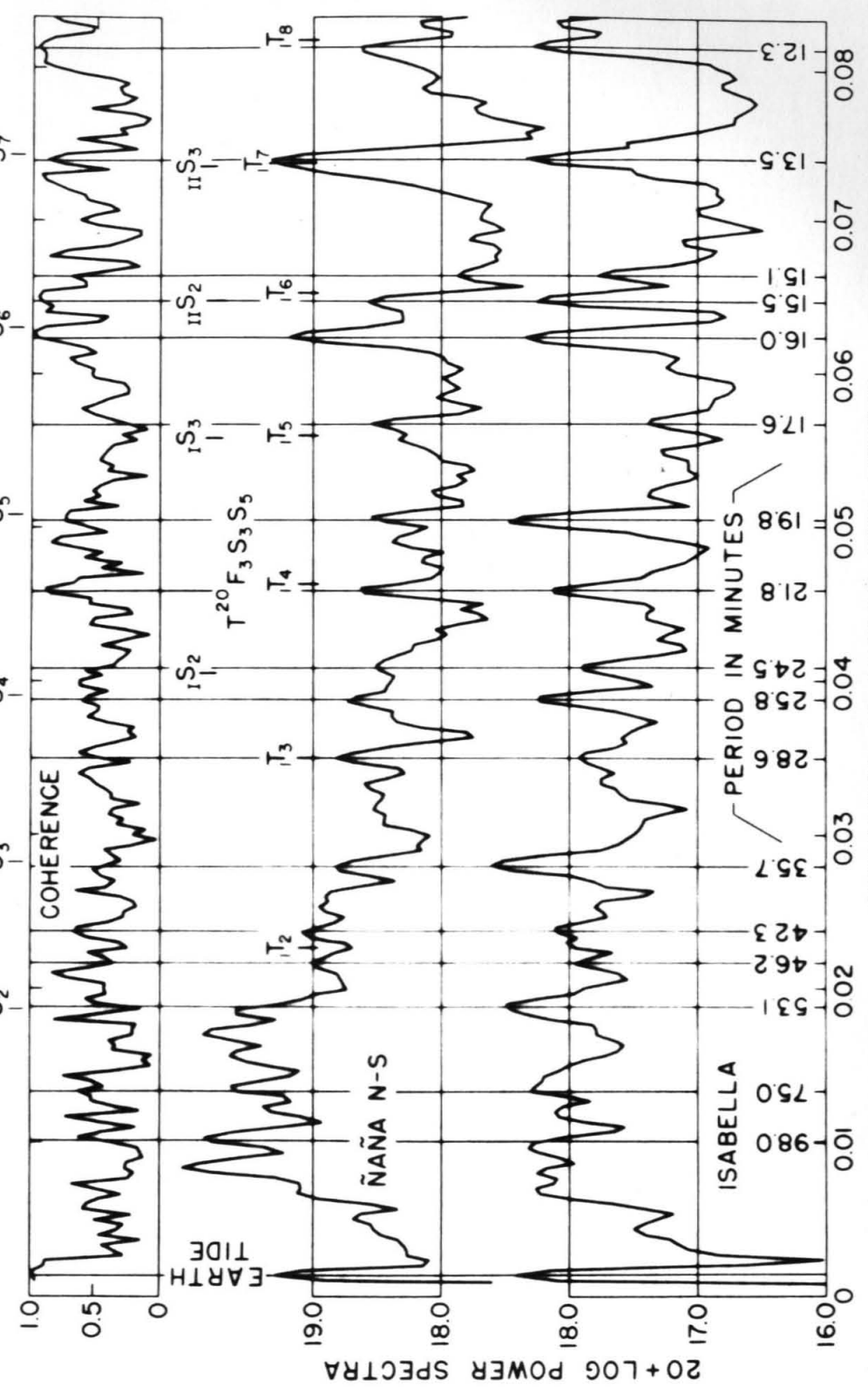
EARTH TIDE
COHERENCE
ÑAÑA N-S
ISABELLA
$T^{20}F_3S_3S_5$
S_2 S_3 S_4 S_5 S_6 S_7
$_IS_2$ $_IS_3$ $_{II}S_2$ $_{II}S_3$
$_IT_2$ $_IT_3$ $_IT_4$ $_IT_5$ $_IT_6$ $_IT_7$ $_IT_8$
PERIOD IN MINUTES
1.0
0.5
0
19.0
18.0
18.0
17.0
16.0
20+LOG POWER SPECTRA
0.01
0.02
0.03
0.04
0.05
0.06
0.07
0.08
FREQUENCY IN CYCLES PER MINUTE

FIG. 2

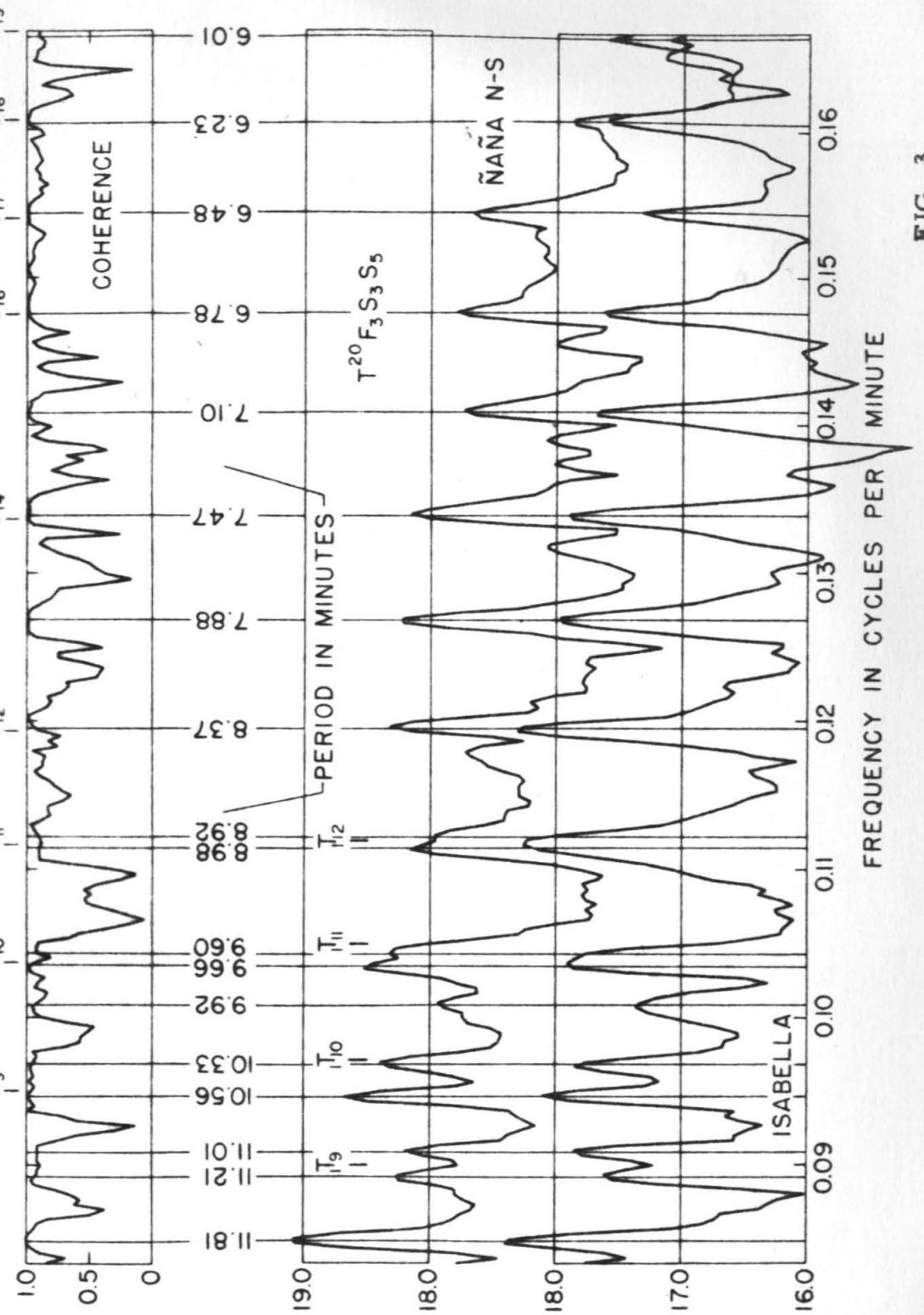
COHERENCE
PERIOD IN MINUTES
$T^{20}F_3S_3S_5$
ÑAÑA N-S
ISABELLA
FREQUENCY IN CYCLES PER MINUTE
S_9 S_{10} S_{11} S_{12} S_{14} S_{16} S_{17} S_{18} S_{19}
T_9 T_{10} T_{11} T_{12}
11.81 11.21 11.01 10.56 10.33 9.92 9.66 9.60 8.98 8.92 8.37 7.88 7.47 7.10 6.78 6.48 6.23 6.01
1.0 0.5 0
19.0 18.0 18.0 17.0 16.0
0.09 0.10 0.11 0.12 0.13 0.14 0.15 0.16

FIG. 3

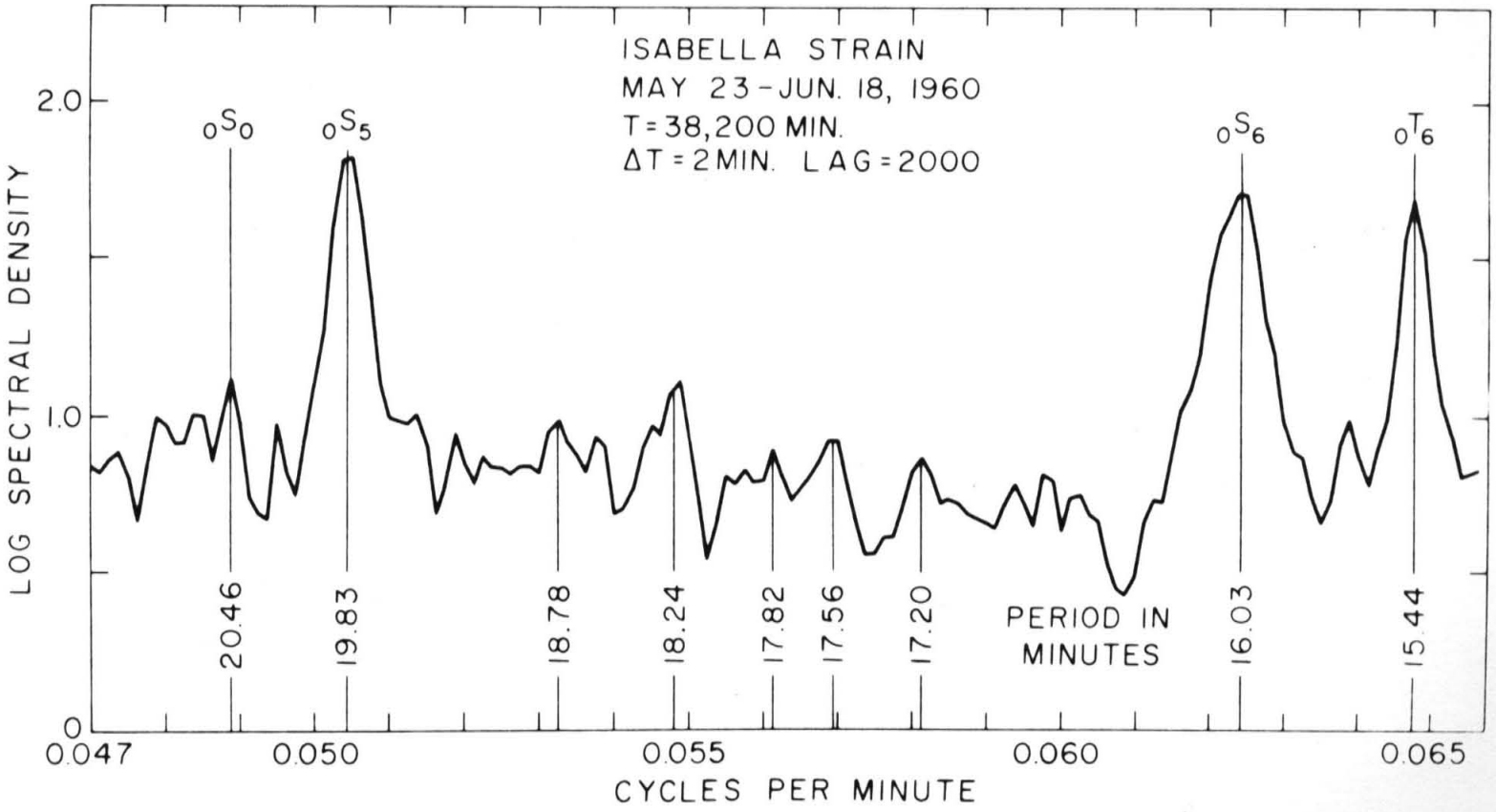
ISABELLA STRAIN
MAY 23 - JUN. 18, 1960
T = 38,200 MIN.
ΔT = 2 MIN. LAG = 2000
$_0S_0$
$_0S_5$
$_0S_6$
$_0T_6$
LOG SPECTRAL DENSITY
2.0
1.0
0
20.46
19.83
18.78
18.24
17.82
17.56
17.20
PERIOD IN MINUTES
16.03
15.44
0.047
0.050
0.055
0.060
0.065
CYCLES PER MINUTE

FIG. 3a

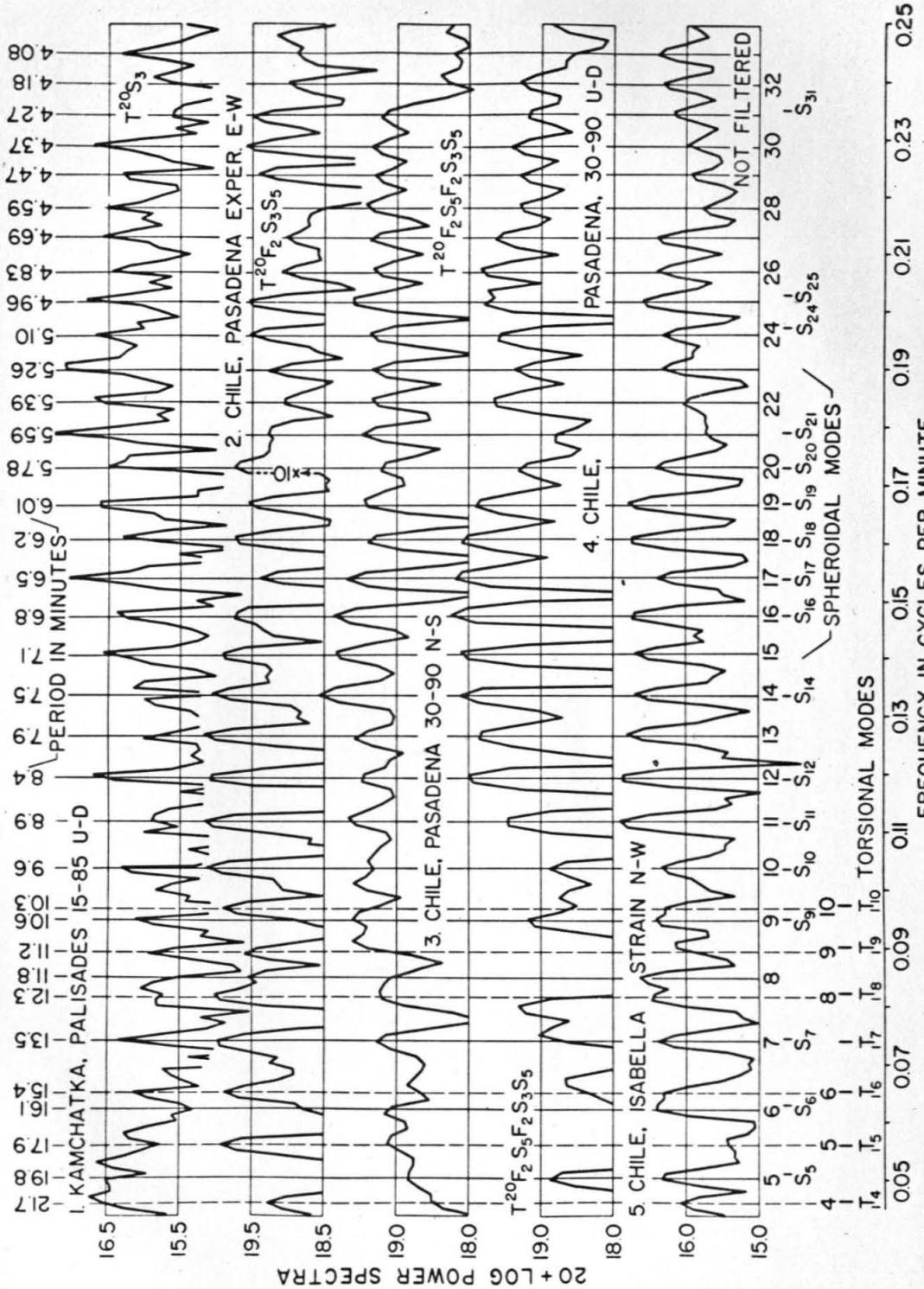
1. KAMCHATKA, PALISADES 15-85 U-D
2. CHILE, PASADENA EXPER. E-W
3. CHILE, PASADENA 30-90 N-S
4. CHILE, PASADENA, 30-90 U-D
5. CHILE, ISABELLA STRAIN N-W
NOT FILTERED
PERIOD IN MINUTES
20 + LOG POWER SPECTRA
FREQUENCY IN CYCLES PER MINUTE
SPHEROIDAL MODES
TORSIONAL MODES

FIG. 4

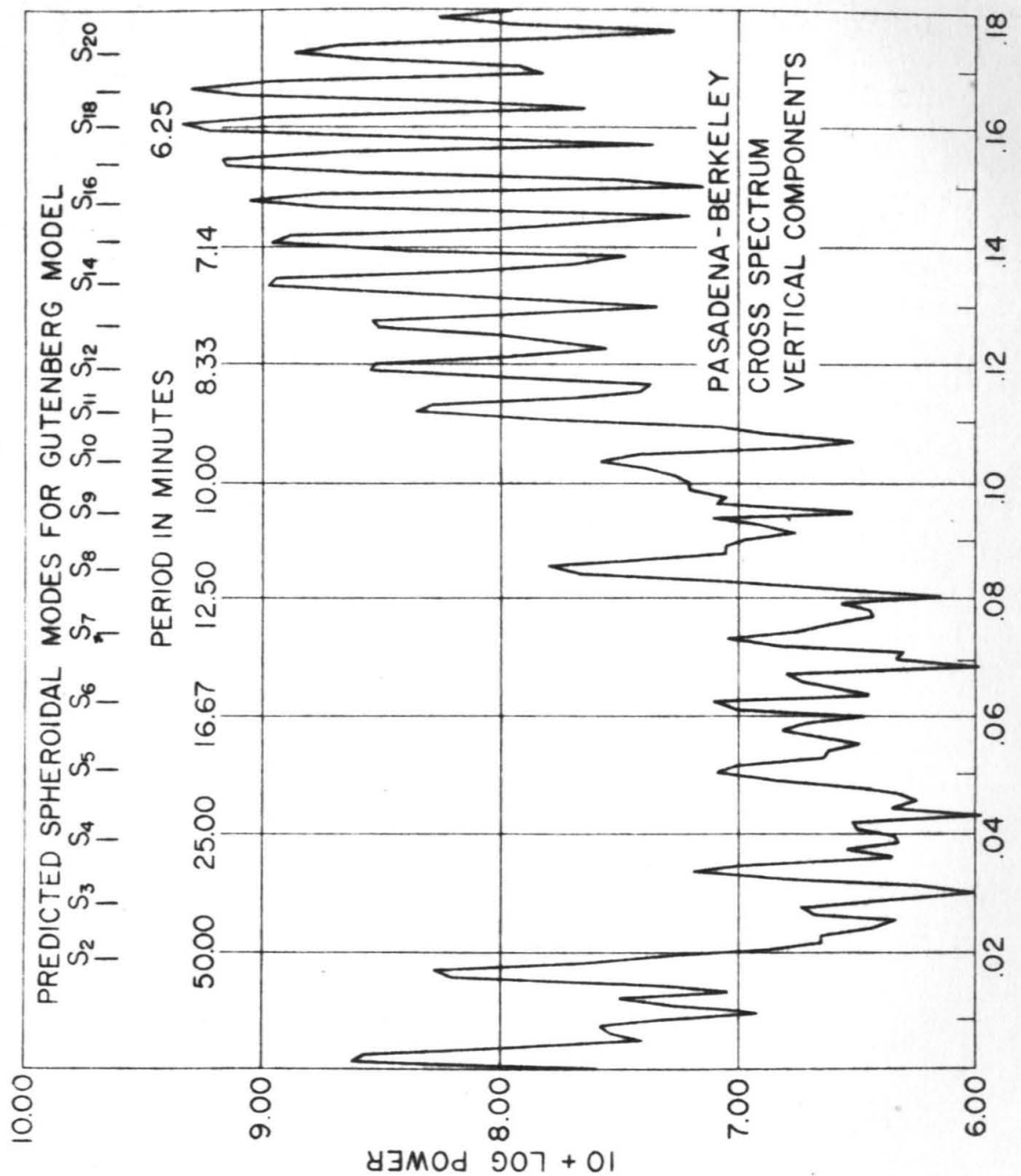
PREDICTED SPHEROIDAL MODES FOR GUTENBERG MODEL
S_2 S_3 S_4 S_5 S_6 S_7 S_8 S_9 S_{10} S_{11} S_{12} S_{14} S_{16} S_{18} S_{20}
PERIOD IN MINUTES
50.00 25.00 16.67 12.50 10.00 8.33 7.14 6.25
PASADENA-BERKELEY
CROSS SPECTRUM
VERTICAL COMPONENTS
10.00
9.00
8.00
7.00
6.00
10 + LOG POWER
.02 .04 .06 .08 .10 .12 .14 .16 .18
FREQUENCY IN CYCLES PER MINUTE

FIG. 5

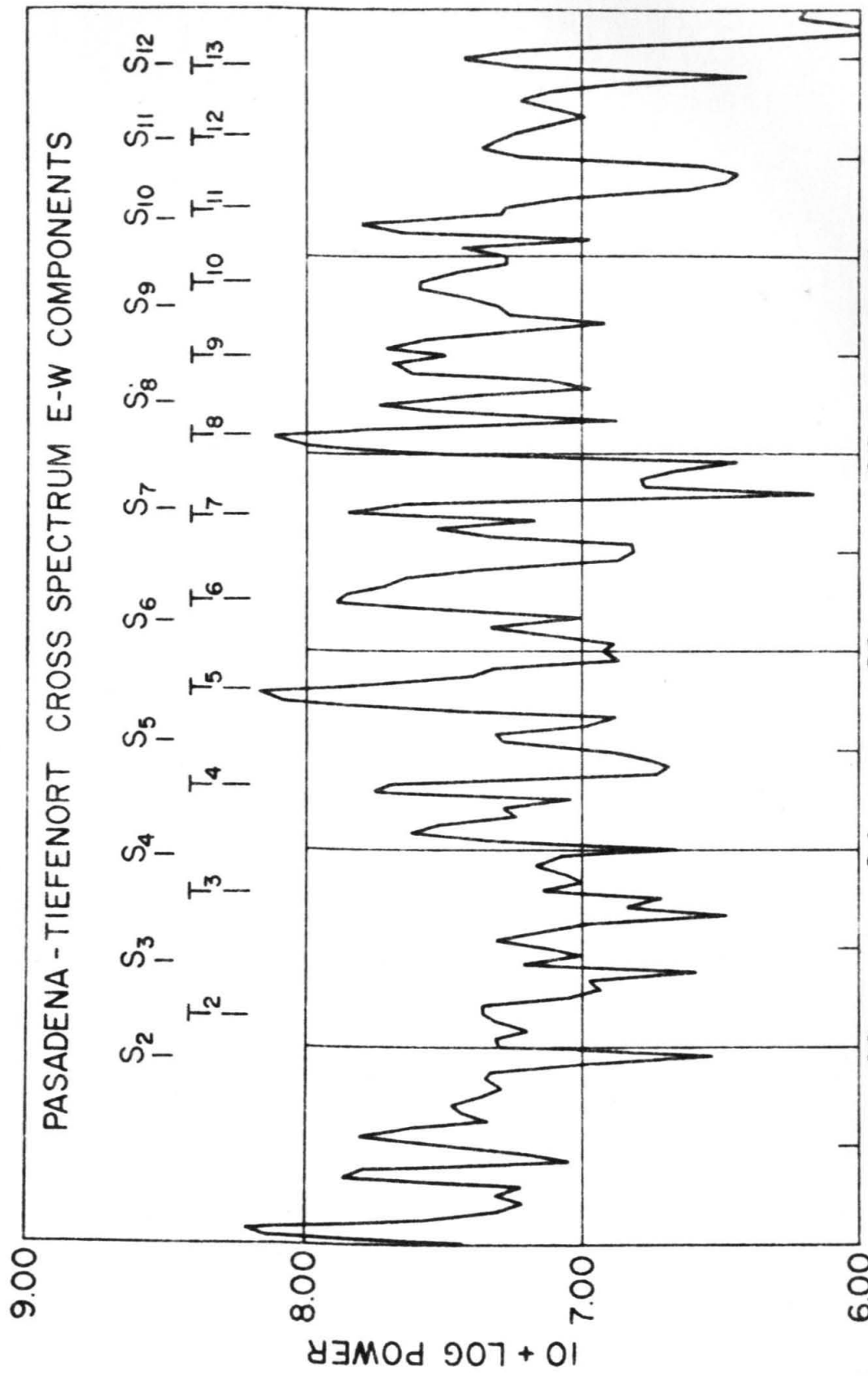
PASADENA - TIEFENORT CROSS SPECTRUM E-W COMPONENTS
S2 S3 S4 S5 S6 S7 S8 S9 S10 S11 S12
T2 T3 T4 T5 T6 T7 T8 T9 T10 T11 T12 T13
9.00
8.00
7.00
6.00
10 + LOG POWER
.02
.04
.06
.08
.10
FREQUENCY IN CYCLES PER MINUTE

FIG. 6

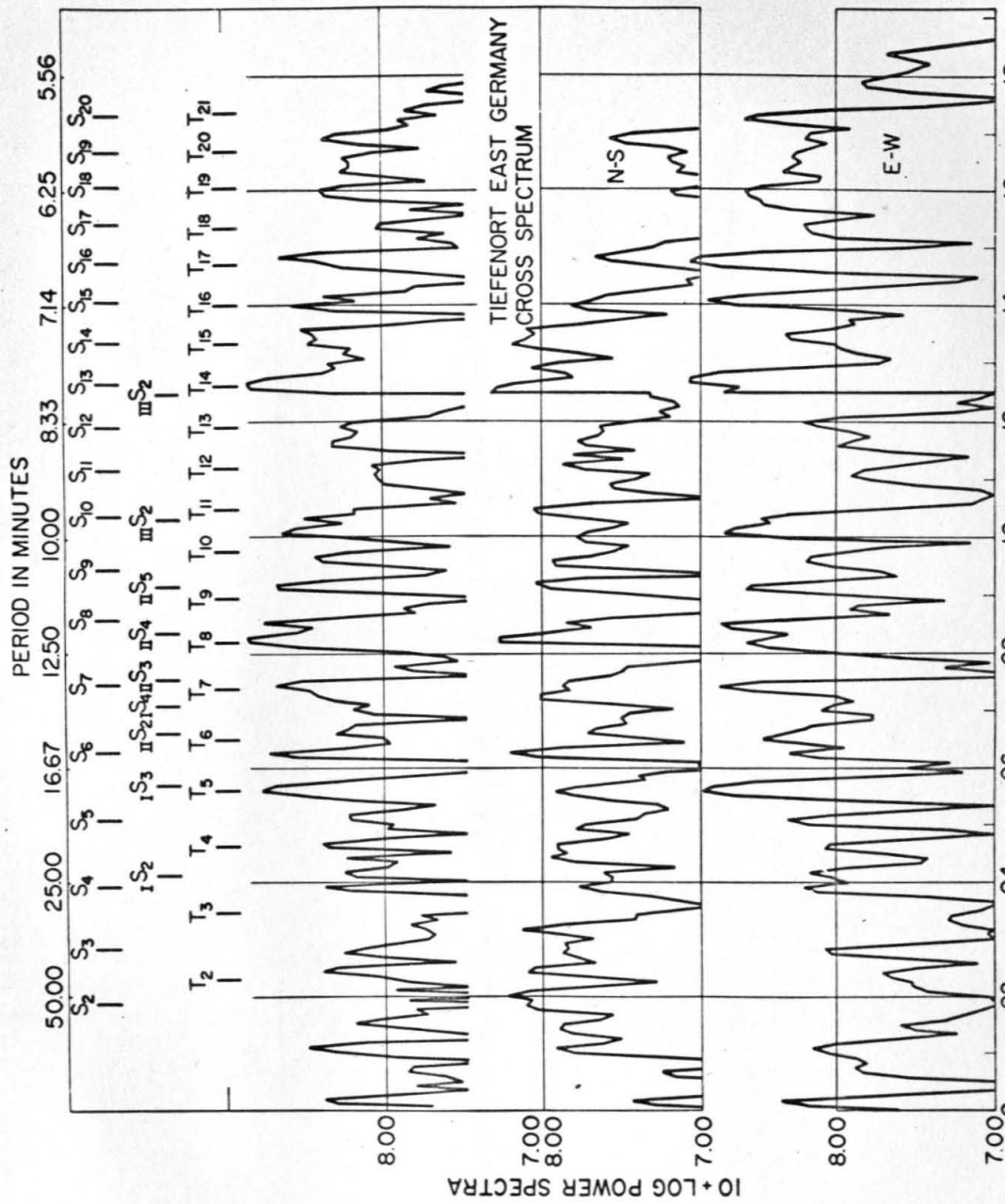
PERIOD IN MINUTES
50.00
25.00
16.67
12.50
10.00
8.33
7.14
6.25
5.56
TIEFENORT EAST GERMANY
CROSS SPECTRUM
N-S
E-W
10 + LOG POWER SPECTRA
8.00
7.00
FREQUENCY IN CYCLES PER MINUTE
0
.02
.04
.06
.08
.10
.12
.14
.16
.18

FIG. 7

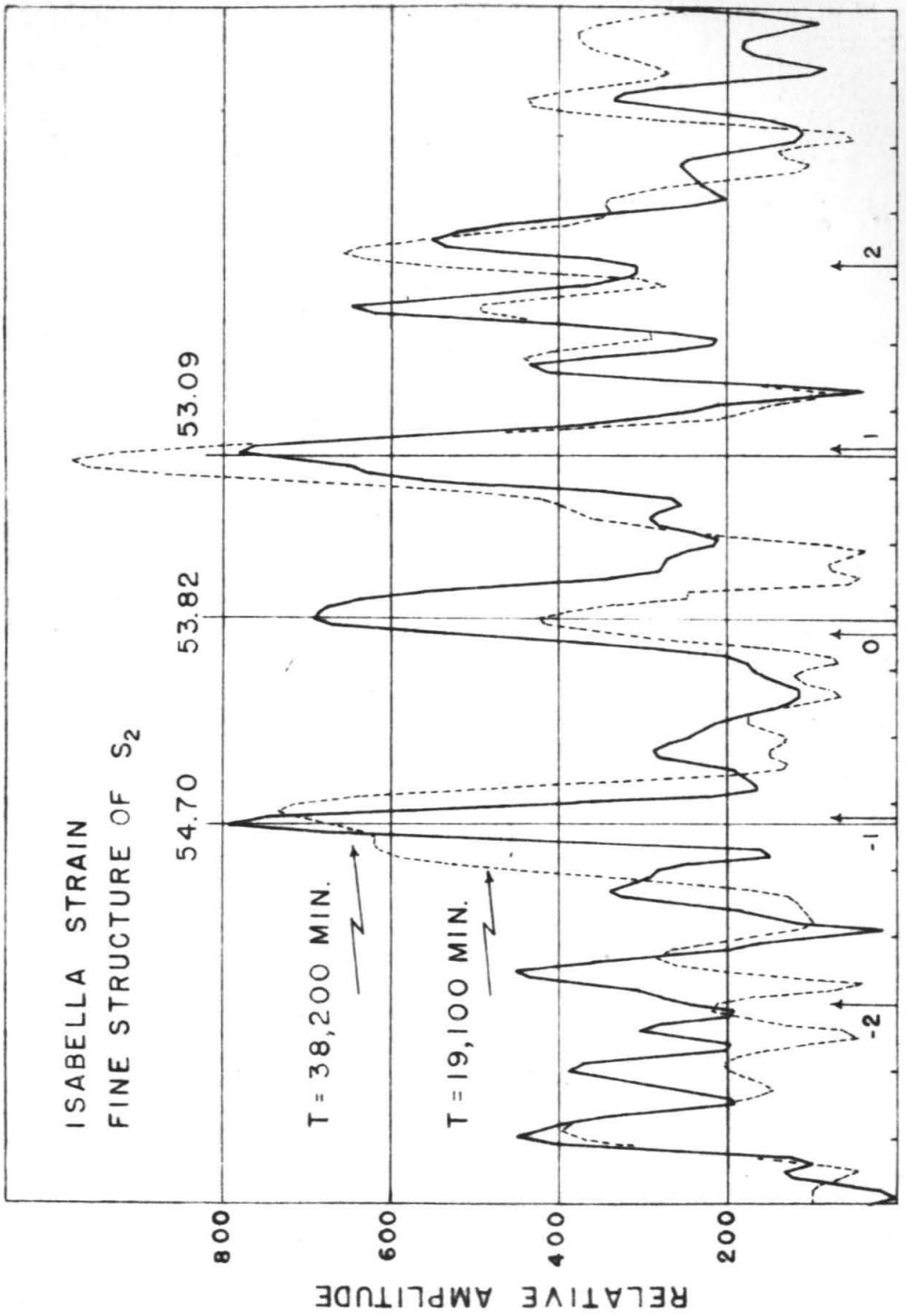
ISABELLA STRAIN
FINE STRUCTURE OF S_2
54.70
53.82
53.09
T = 38,200 MIN.
T = 19,100 MIN.
RELATIVE AMPLITUDE
800
600
400
200
.0178
.0180
.0182
.0184
.0186
.0188
.0190
.0192
.0194
CYCLES PER MINUTE
-2
-1
0
1
2

FIG. 8

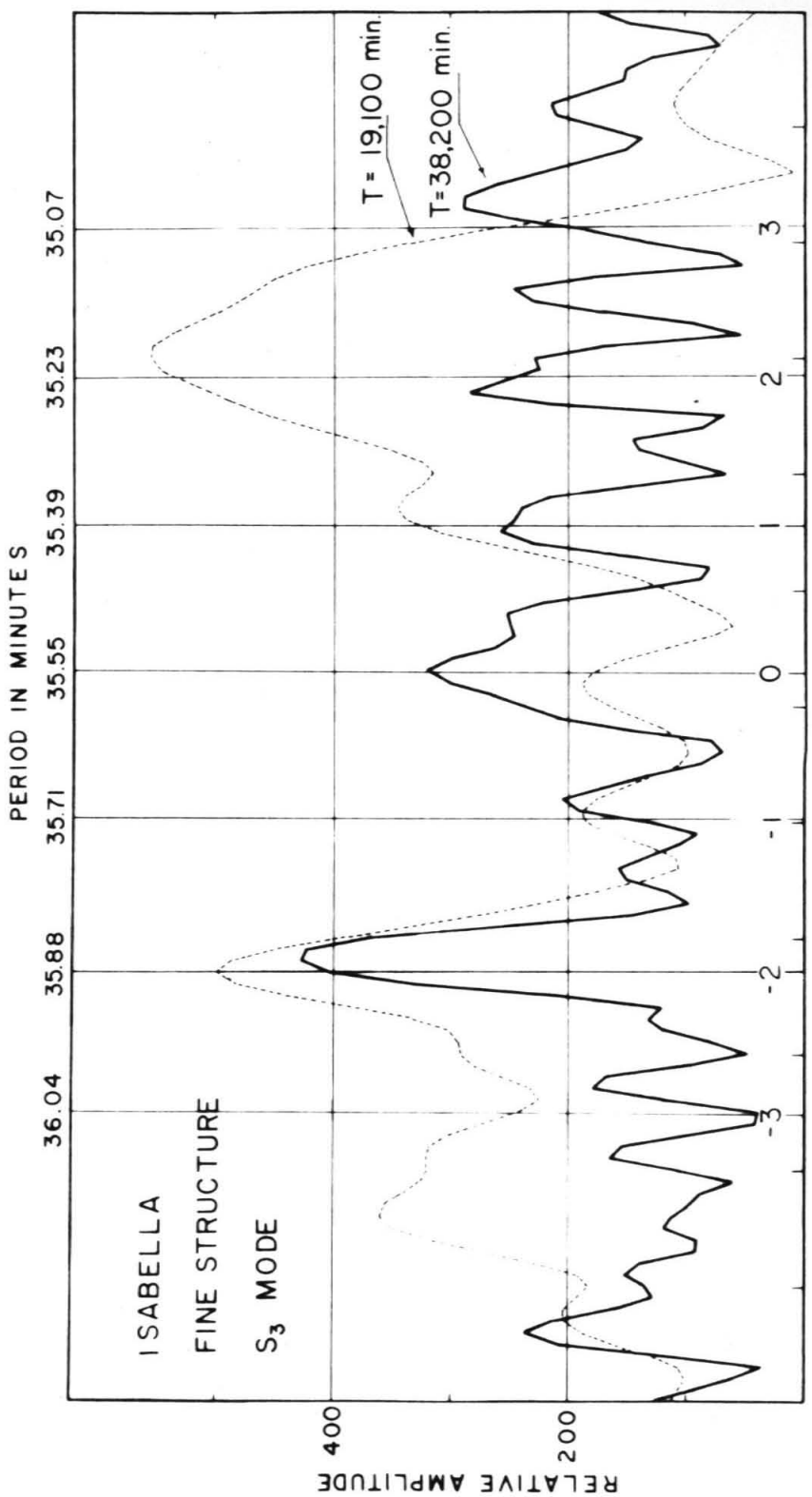
ISABELLA
FINE STRUCTURE
S_3 MODE
T = 19,100 min.
T=38,200 min.
PERIOD IN MINUTES
36.04
35.88
35.71
35.55
35.39
35.23
35.07
CYCLES PER MINUTE
.0276
.0278
.0280
.0282
.0284
.0286
-3
-2
-1
0
1
2
3
RELATIVE AMPLITUDE
200
400

FIG. 9

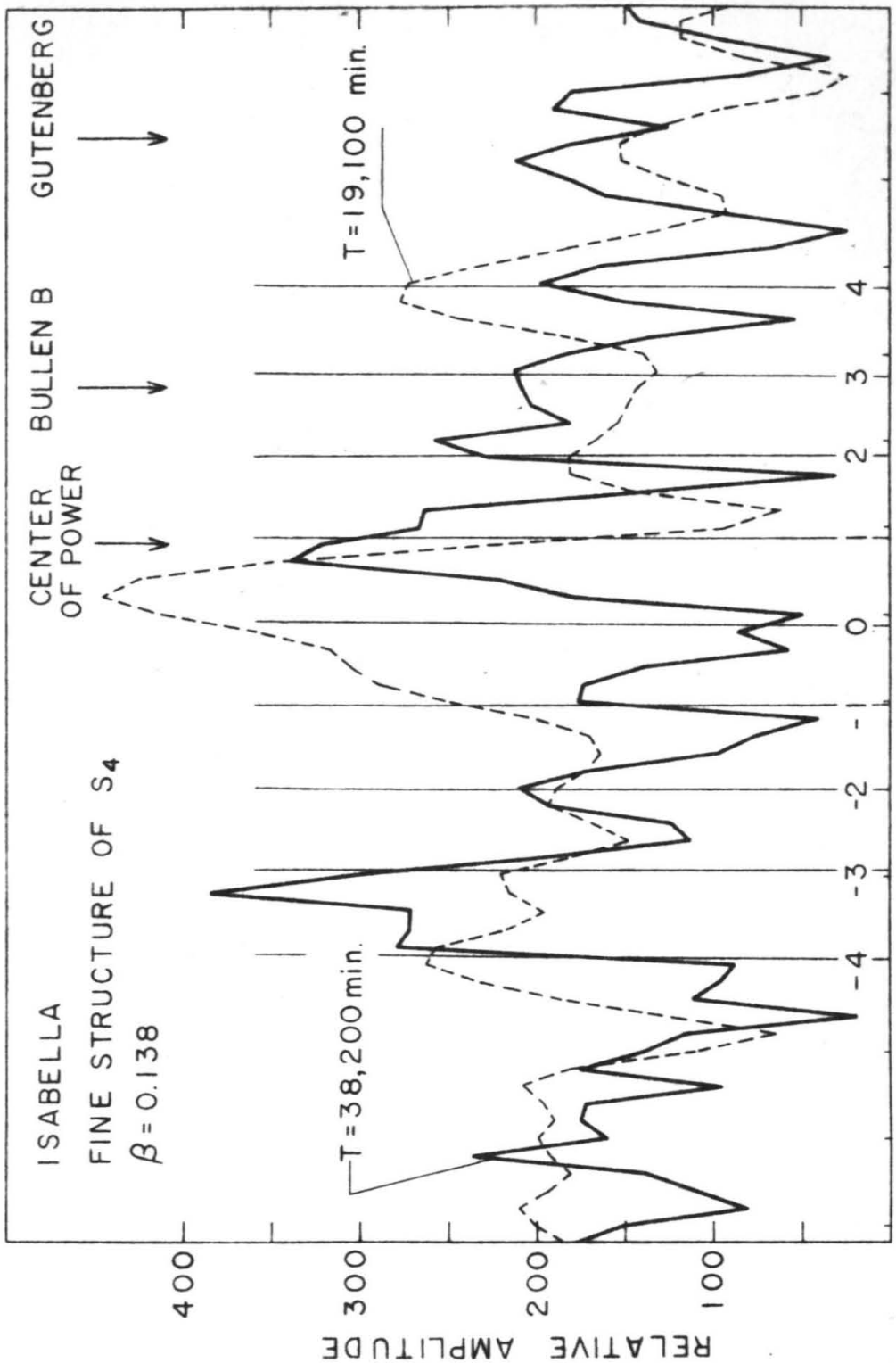
ISABELLA
FINE STRUCTURE OF S_4
$\beta = 0.138$
CENTER OF POWER
BULLEN B
GUTENBERG
T=38,200 min.
T=19,100 min.
RELATIVE AMPLITUDE
400
300
200
100
-4
-3
-2
-1
0
1
2
3
4
.0380
.0384
.0388
.0392
CYCLES PER MINUTE

FIG. 10

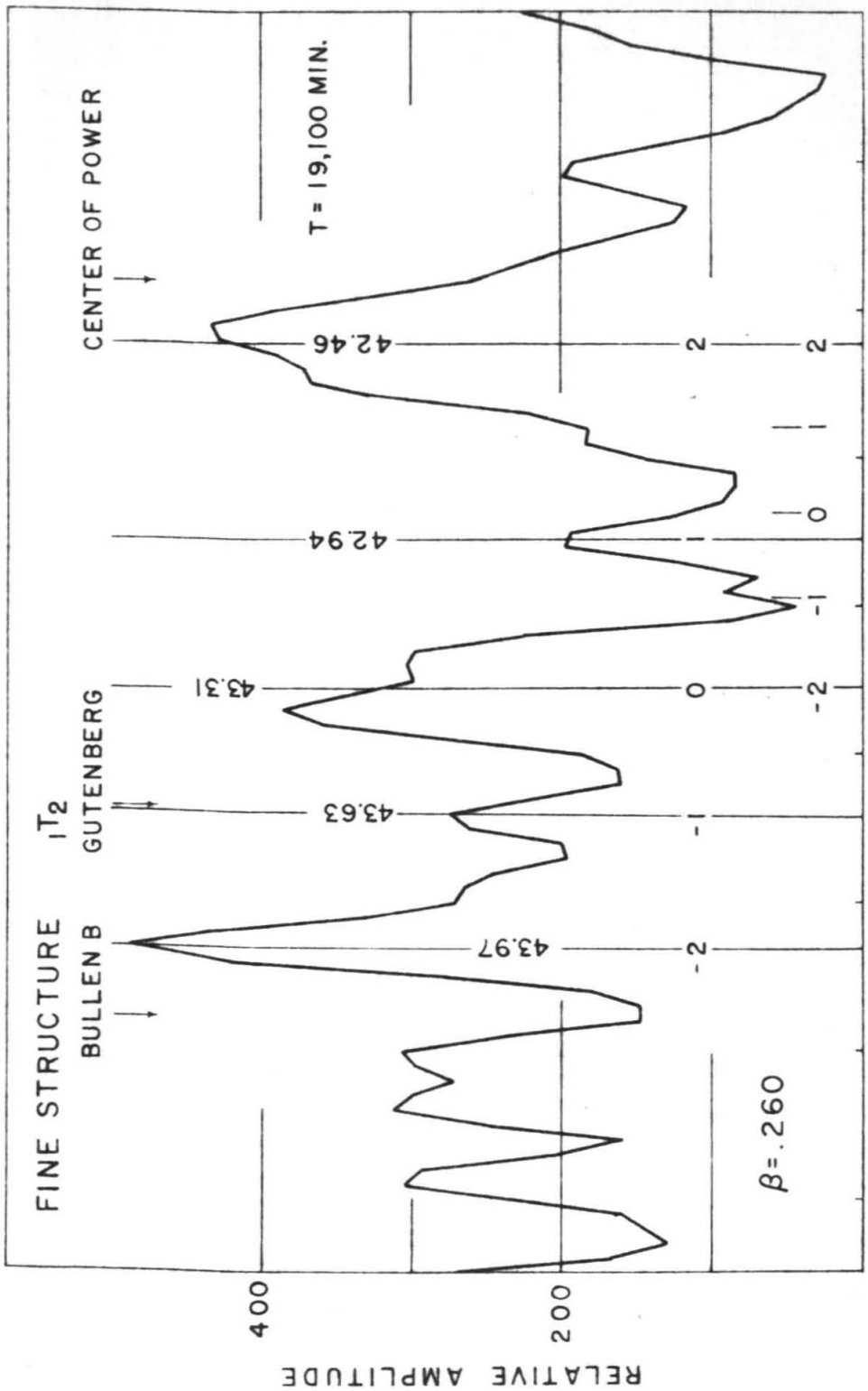
FINE STRUCTURE
BULLEN B
GUTENBERG
$_1T_2$
CENTER OF POWER
T = 19,100 MIN.
43.97
43.63
43.31
42.94
42.46
-2
-1
0
-1
0
1
2
2
β=.260
400
200
RELATIVE AMPLITUDE
.0224
.0228
.0232
.0236
CYCLES PER MINUTE

FIG. 11

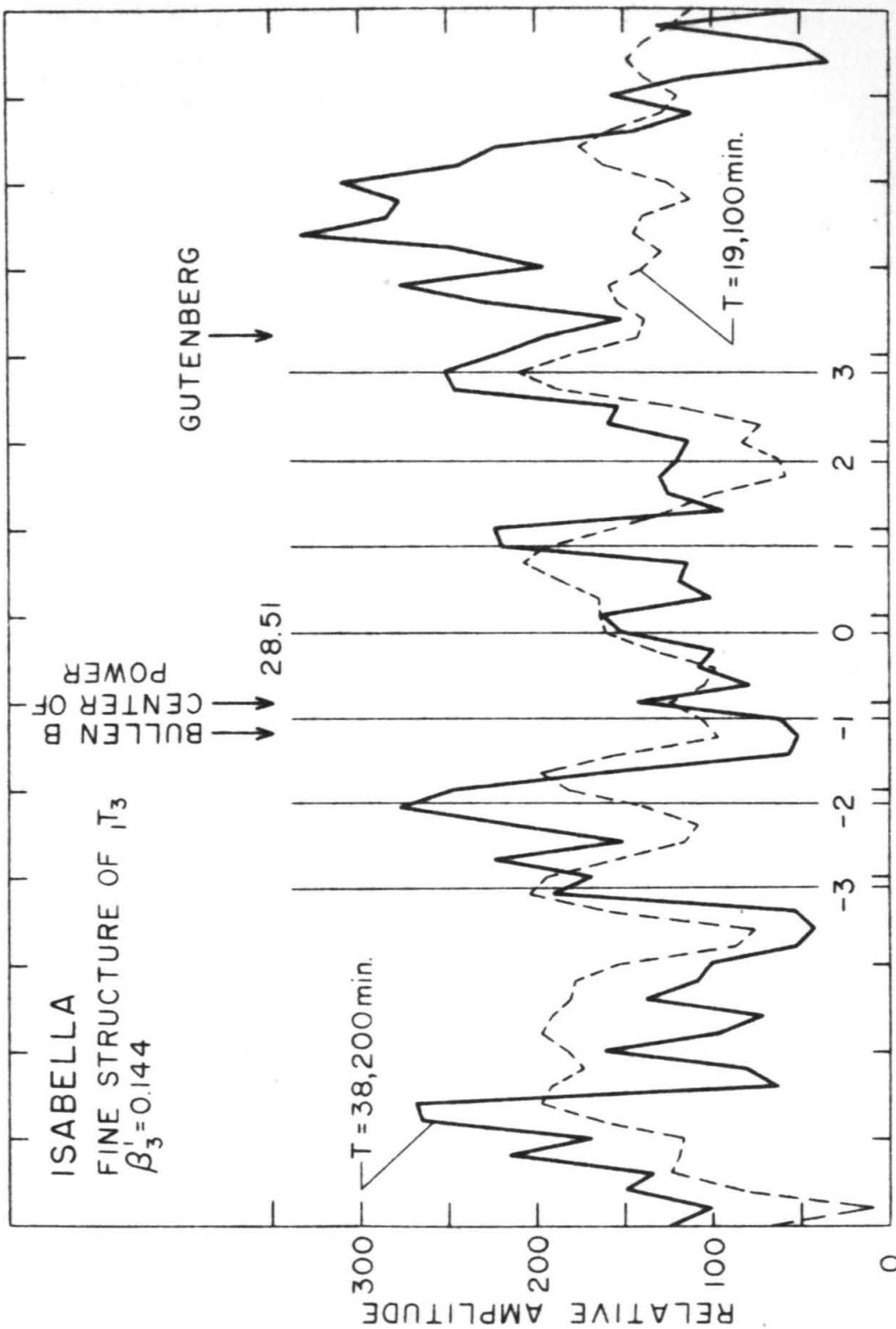
ISABELLA
FINE STRUCTURE OF I_3
$\beta_3'=0.144$
BULLEN B
CENTER OF
POWER
28.51
GUTENBERG
T=38,200min.
T=19,100min.
RELATIVE AMPLITUDE
300
200
100
0
.0344
.0348
.0352
.0356
-3
-2
-1
0
1
2
3
CYCLES PER MINUTE

FIG. 12

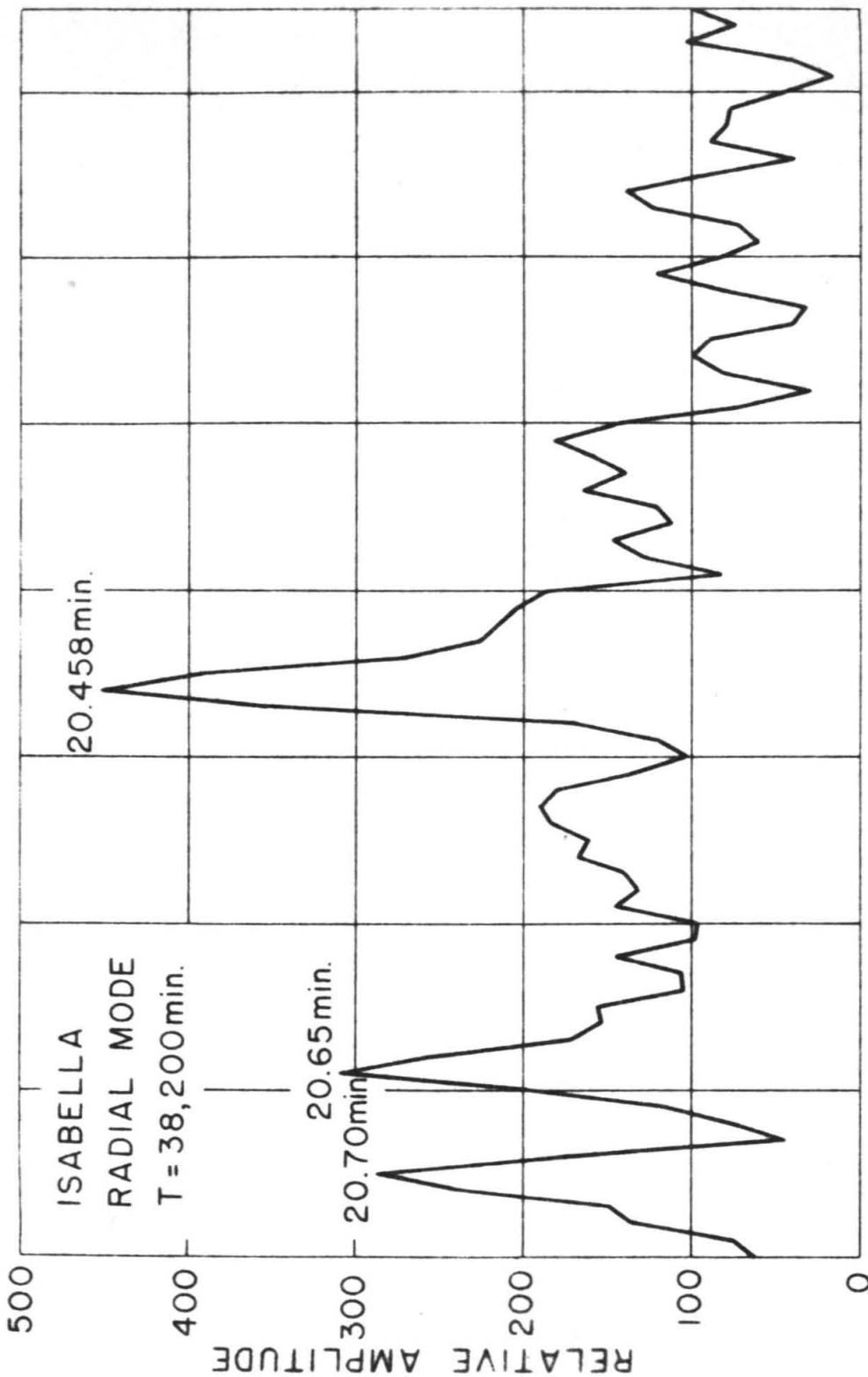
ISABELLA
RADIAL MODE
T = 38,200min.
20.458min.
20.65min.
20.70min
RELATIVE AMPLITUDE
500
400
300
200
100
0
.0482
.0486
.0490
.0494
CYCLES PER MINUTE

FIG. 13

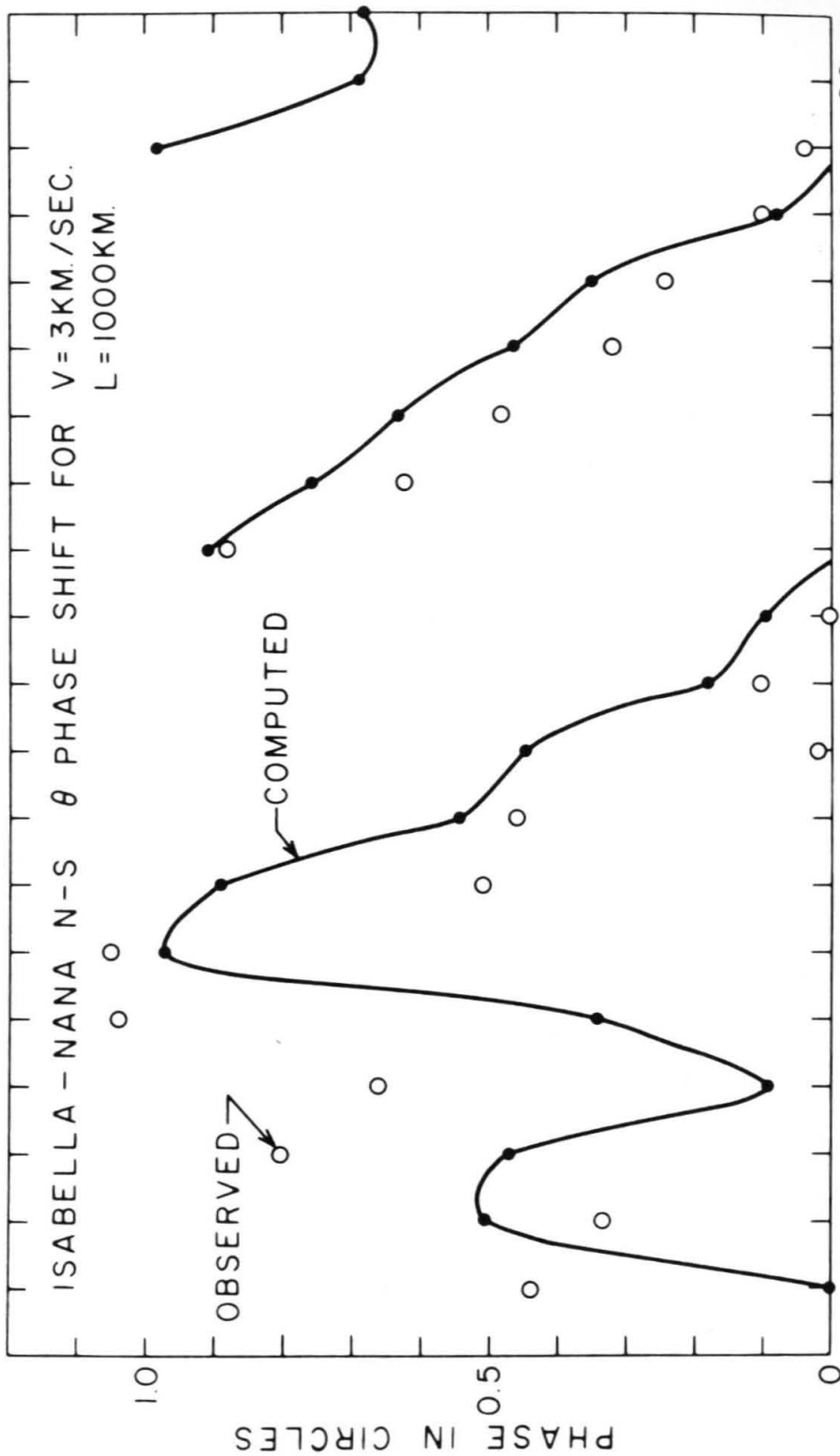
ISABELLA-NANA N-S θ PHASE SHIFT FOR V=3KM./SEC.
L=1000KM.
COMPUTED
OBSERVED
PHASE IN CIRCLES
MODE NUMBER
0
0.5
1.0
2
4
6
8
10
12
14
16
18
20

FIG. 14

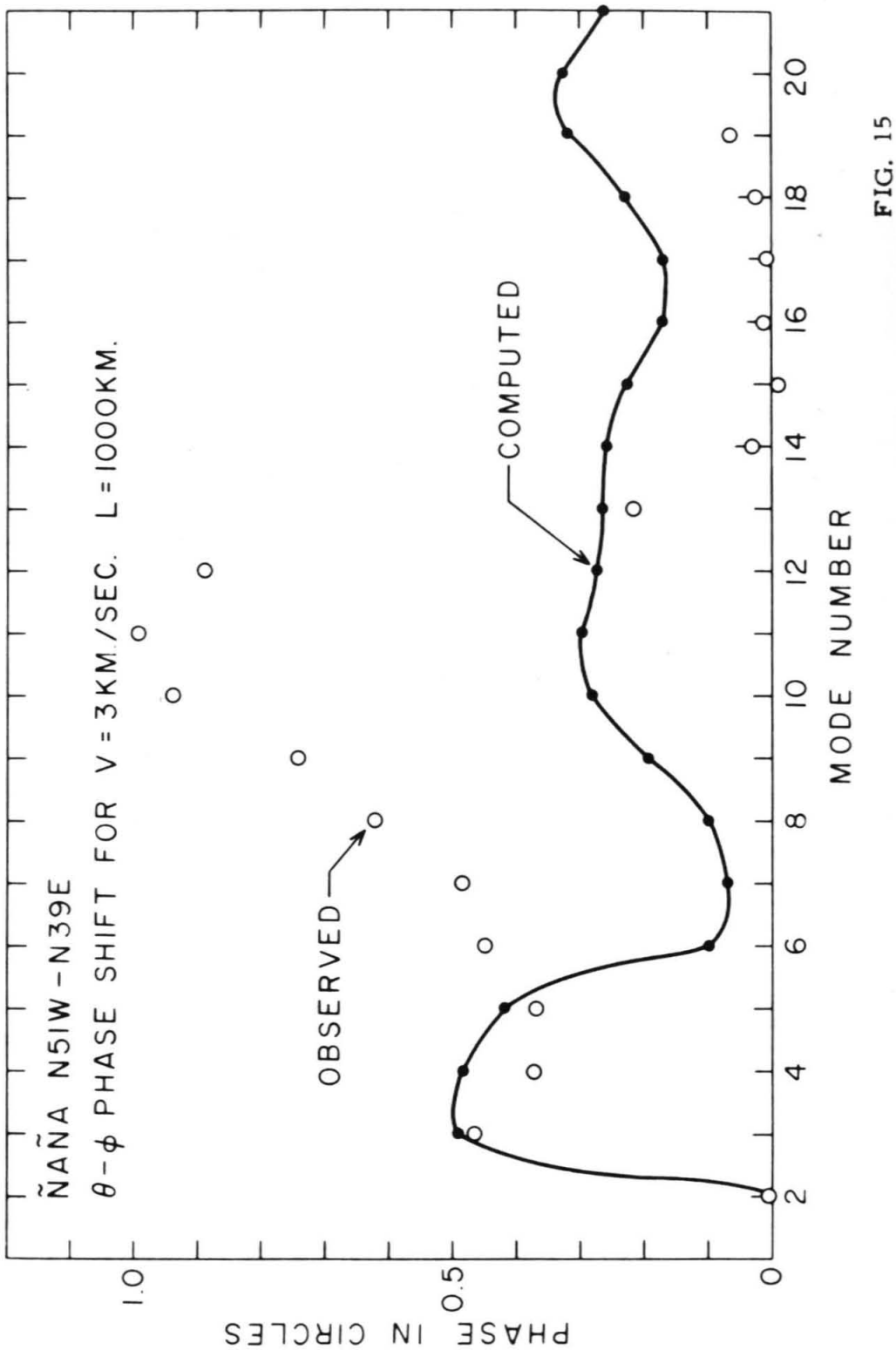
ÑAÑA N51W-N39E
θ-φ PHASE SHIFT FOR V=3KM./SEC. L=1000KM.
OBSERVED
COMPUTED
PHASE IN CIRCLES
MODE NUMBER
0
0.5
1.0
2
4
6
8
10
12
14
16
18
20

FIG. 15

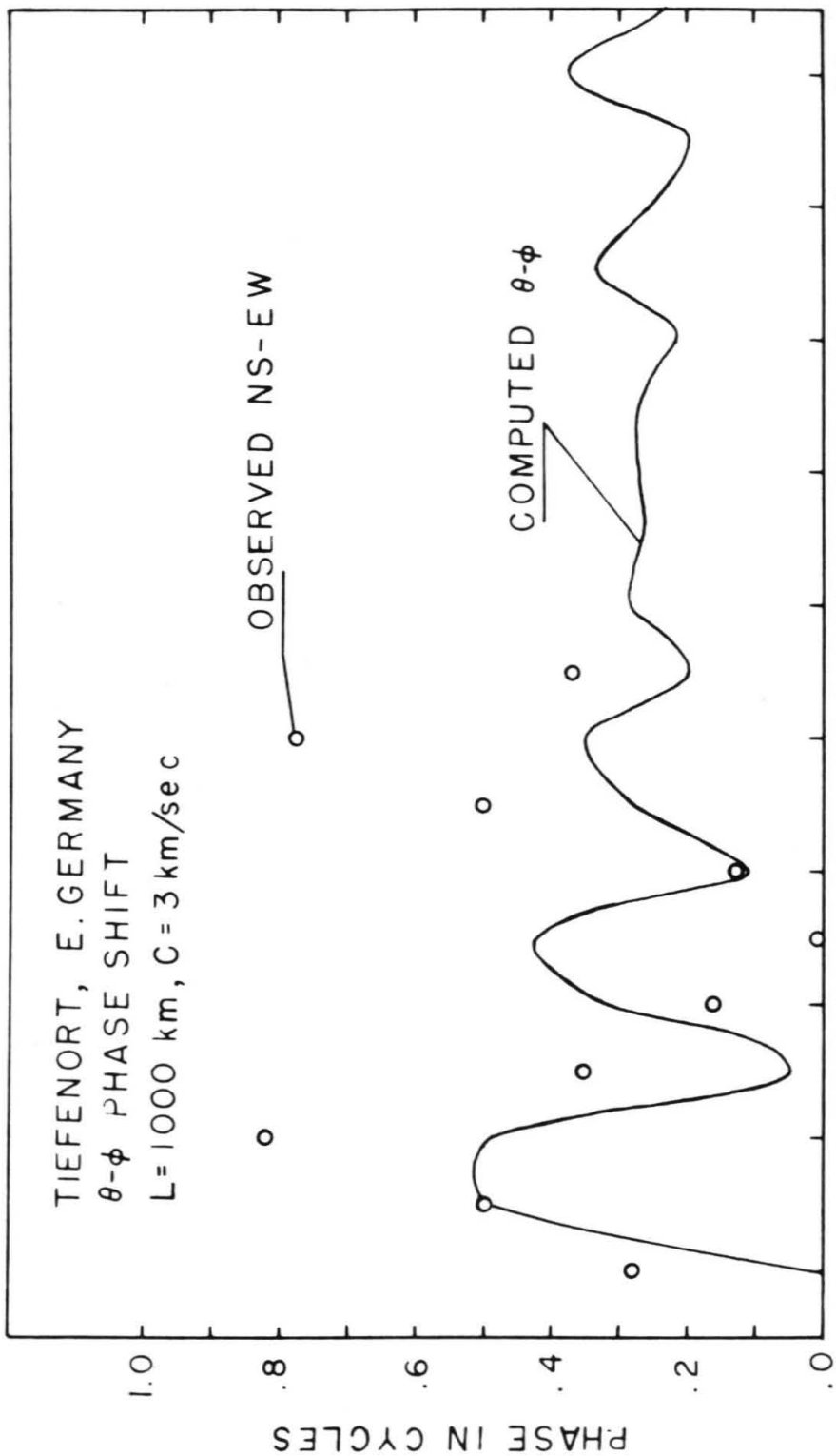
TIEFENORT, E. GERMANY
θ-φ PHASE SHIFT
L= 1000 km, C= 3 km/sec
OBSERVED NS-EW
COMPUTED θ-φ
PHASE IN CYCLES
MODE NUMBER
.0
.2
.4
.6
.8
1.0
2
4
6
8
10
12
14
16
18
20

FIG. 16

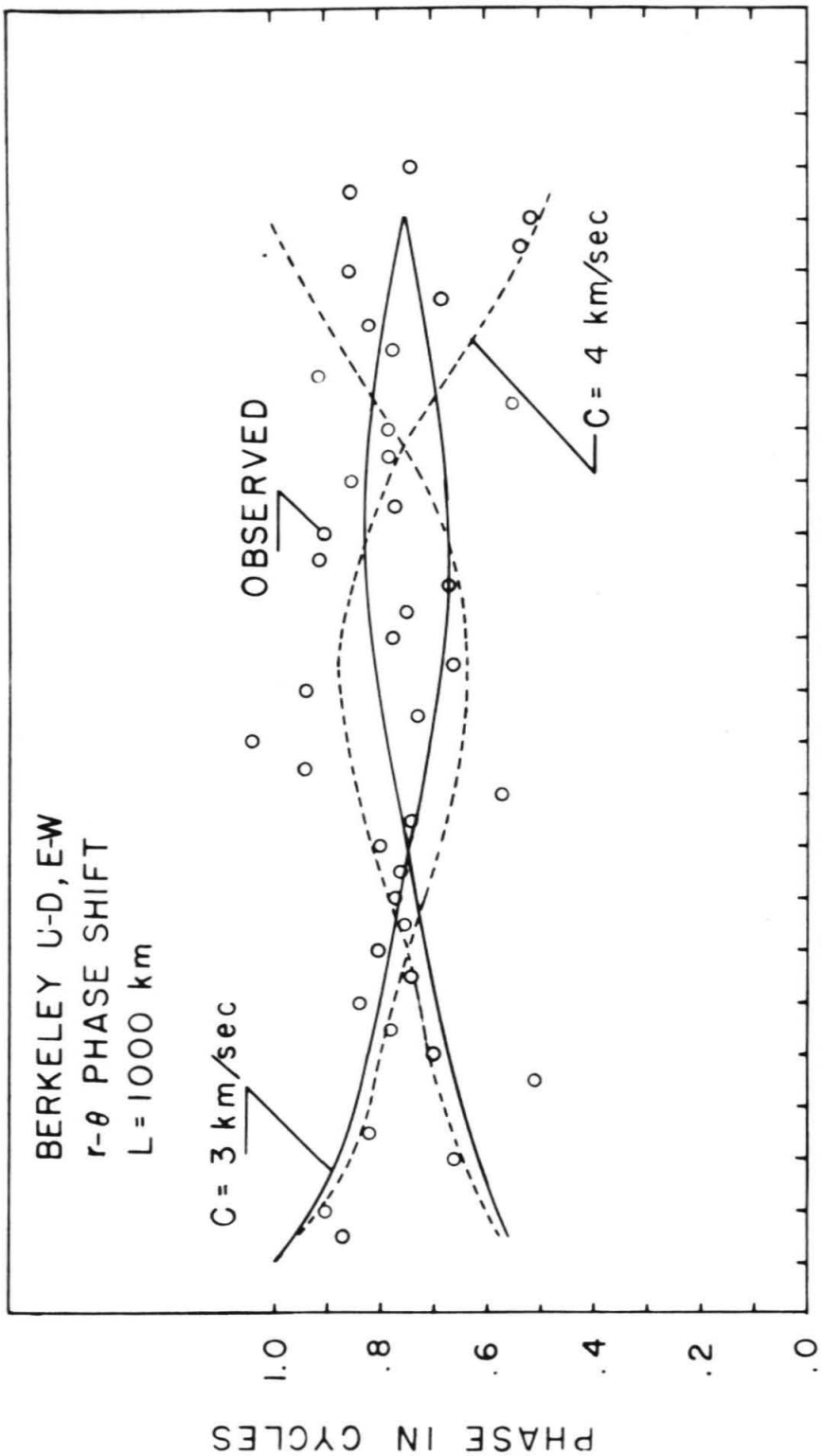
BERKELEY U-D, E-W
r-θ PHASE SHIFT
L = 1000 km
C = 3 km/sec
OBSERVED
C = 4 km/sec
PHASE IN CYCLES
MODE NUMBER
0.0
.2
.4
.6
.8
1.0
2
6
10
14
18
22
26
30
34
38
42
46

FIG. 17

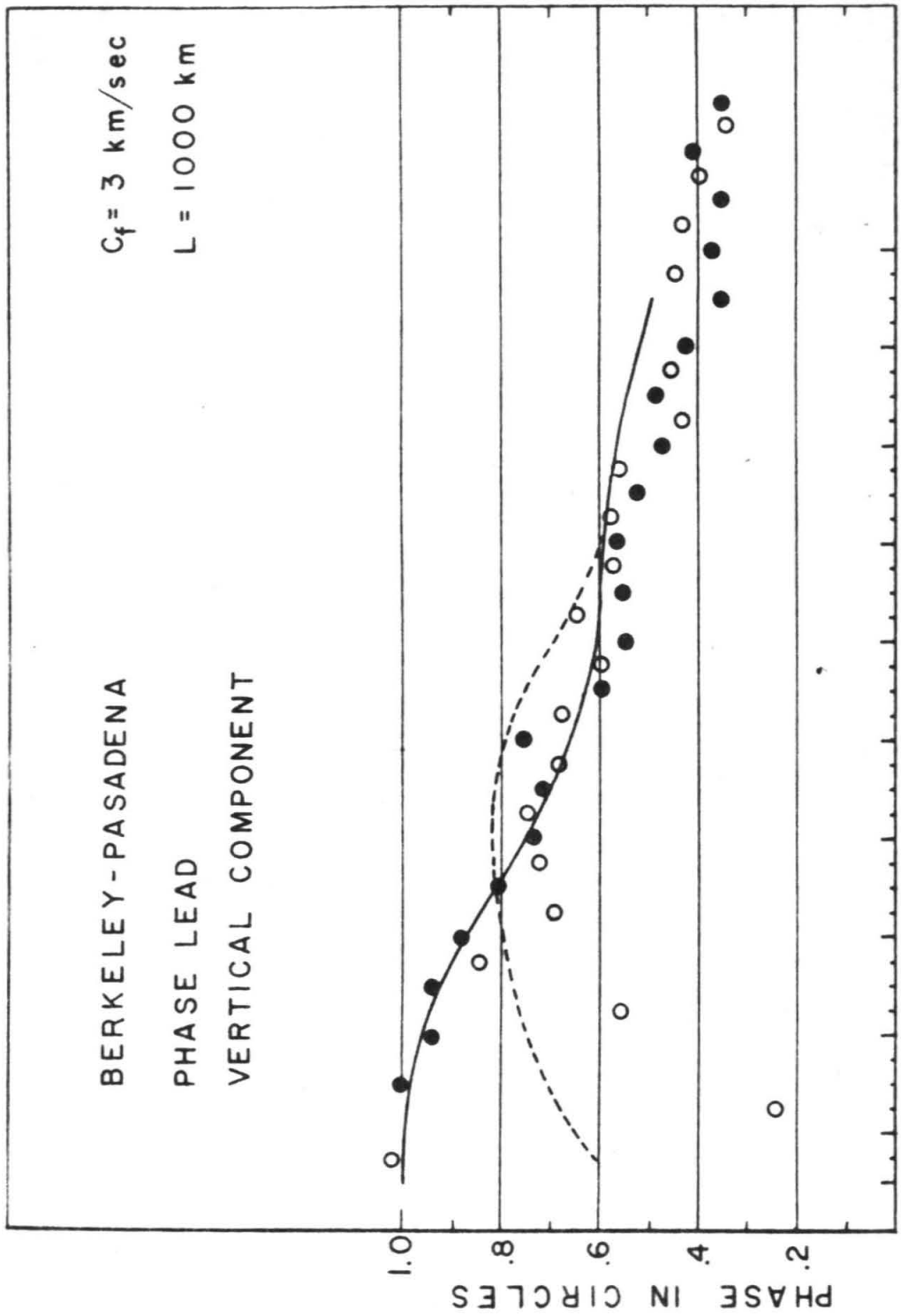
BERKELEY-PASADENA
PHASE LEAD
VERTICAL COMPONENT
C_f = 3 km/sec
L = 1000 km
PHASE IN CIRCLES
1.0
.8
.6
.4
.2
4
8
12
16
20
24
28
32
36
40
SPHEROIDAL MODE NUMBER

FIG. 18

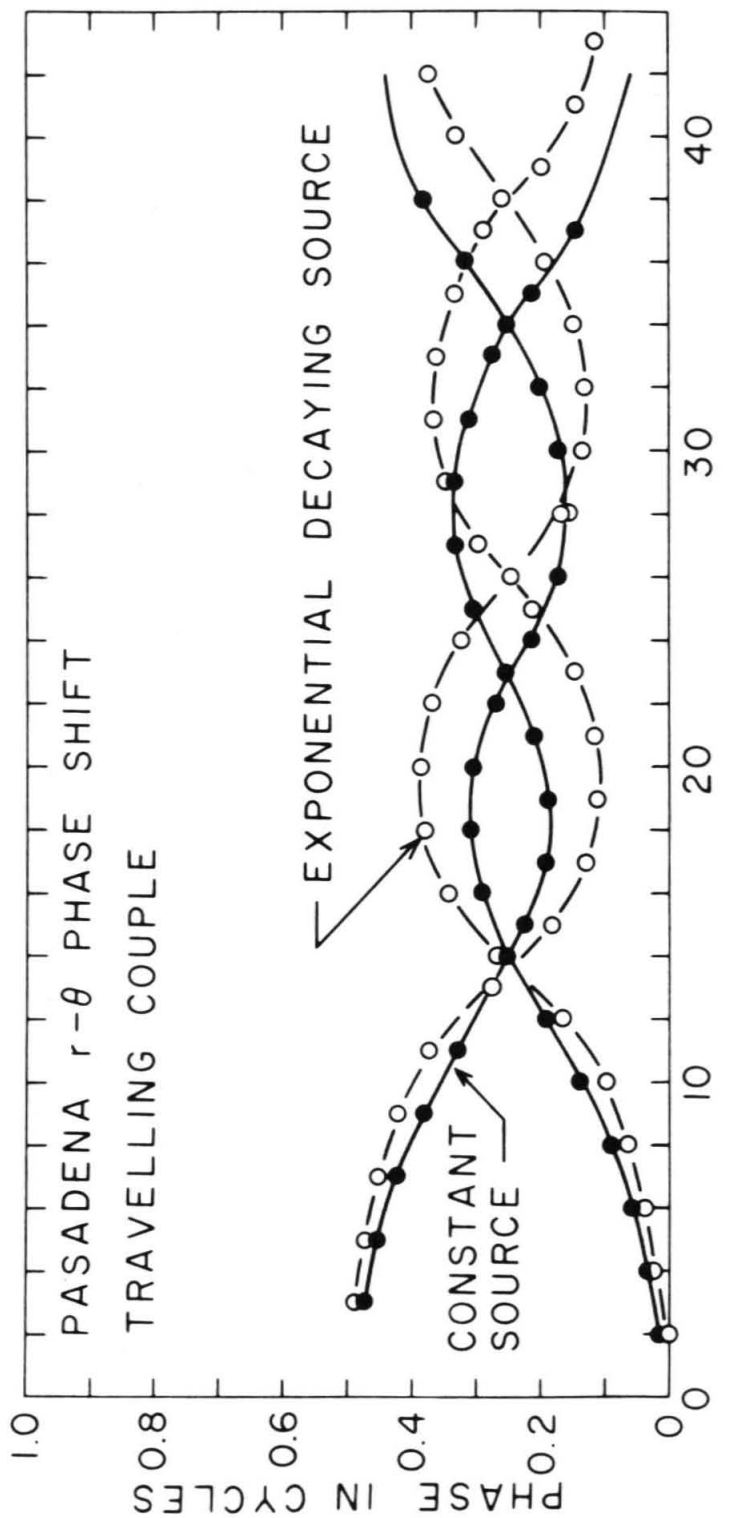
PASADENA r-θ PHASE SHIFT
TRAVELLING COUPLE
EXPONENTIAL DECAYING SOURCE
CONSTANT SOURCE
PHASE IN CYCLES
MODE NUMBER
0
0.2
0.4
0.6
0.8
1.0
10
20
30
40

FIG. 19

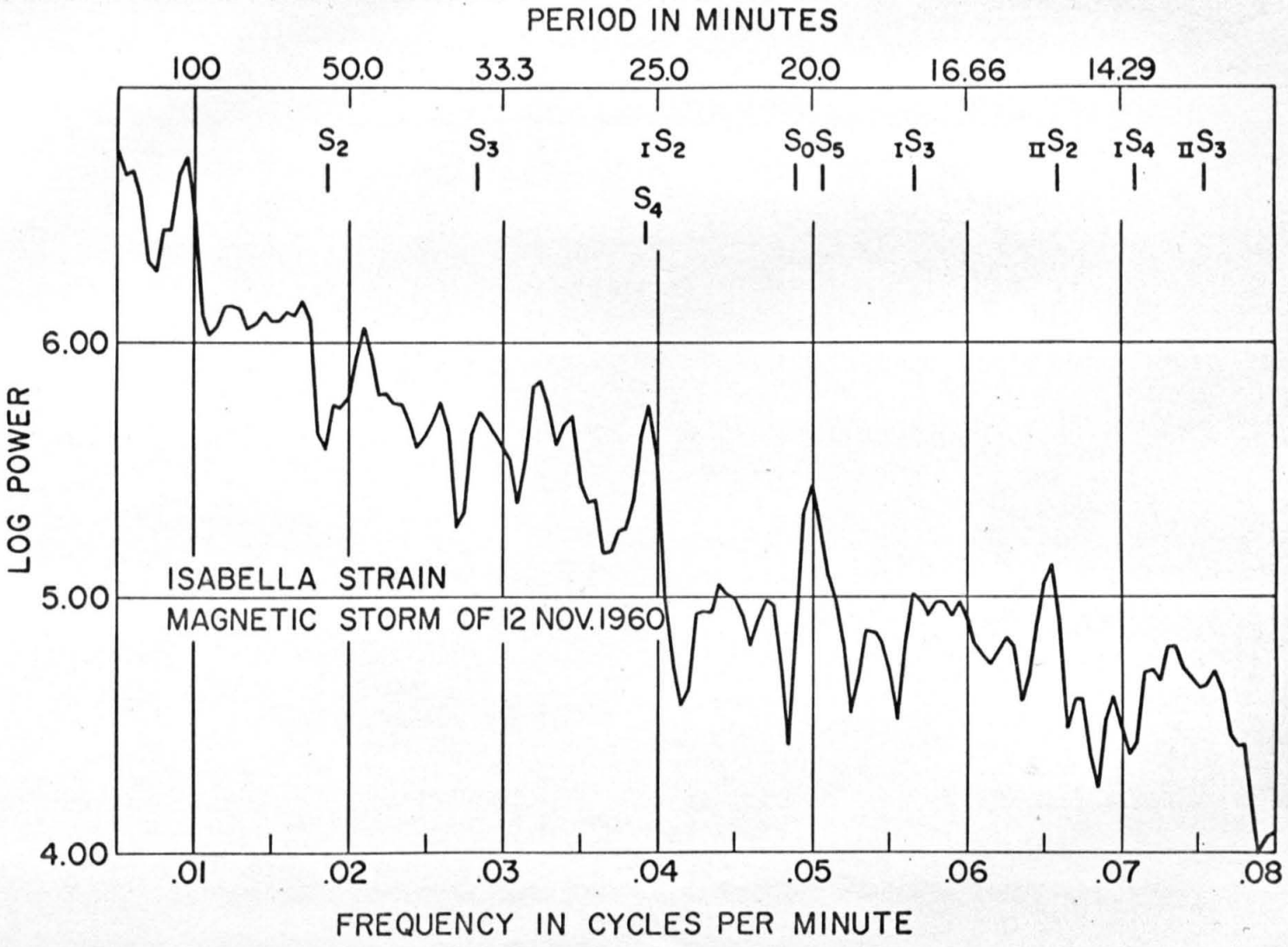
PERIOD IN MINUTES
100
50.0
33.3
25.0
20.0
16.66
14.29
S2
S3
IS2
S4
S0S5
IS3
IIS2
IS4
IIS3
LOG POWER
6.00
5.00
4.00
ISABELLA STRAIN
MAGNETIC STORM OF 12 NOV. 1960
.01
.02
.03
.04
.05
.06
.07
.08
FREQUENCY IN CYCLES PER MINUTE

FIG. 20

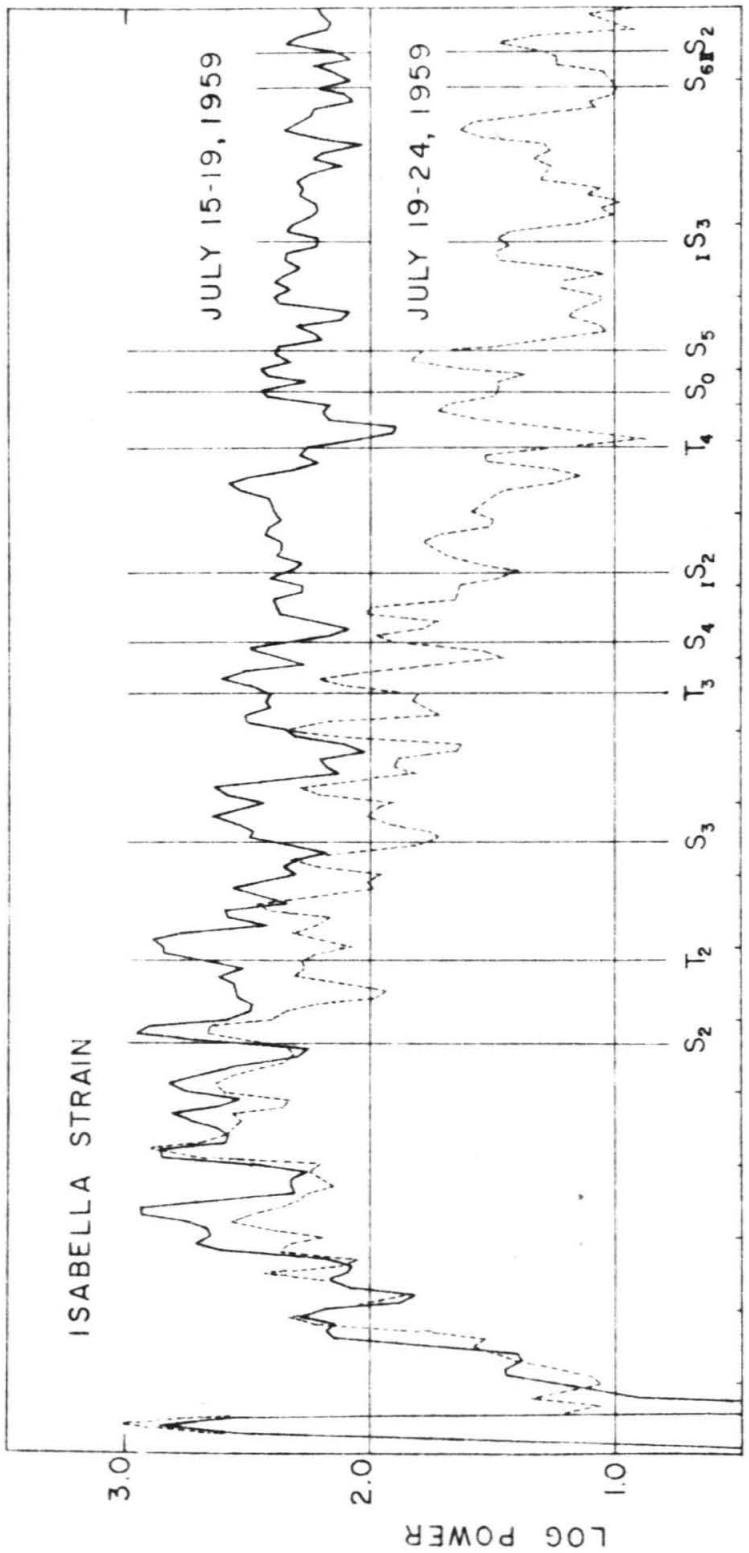
ISABELLA STRAIN
JULY 15-19, 1959
JULY 19-24, 1959
LOG POWER
3.0
2.0
1.0
.4
.8
1.2
1.6
2.0
2.4
2.6
3.0
3.4
CYCLES PER HOUR
S_2 T_2 S_3 T_3 S_4 $_1S_2$ T_4 S_0 S_5 $_1S_3$ S_6P_2

FIG. 21

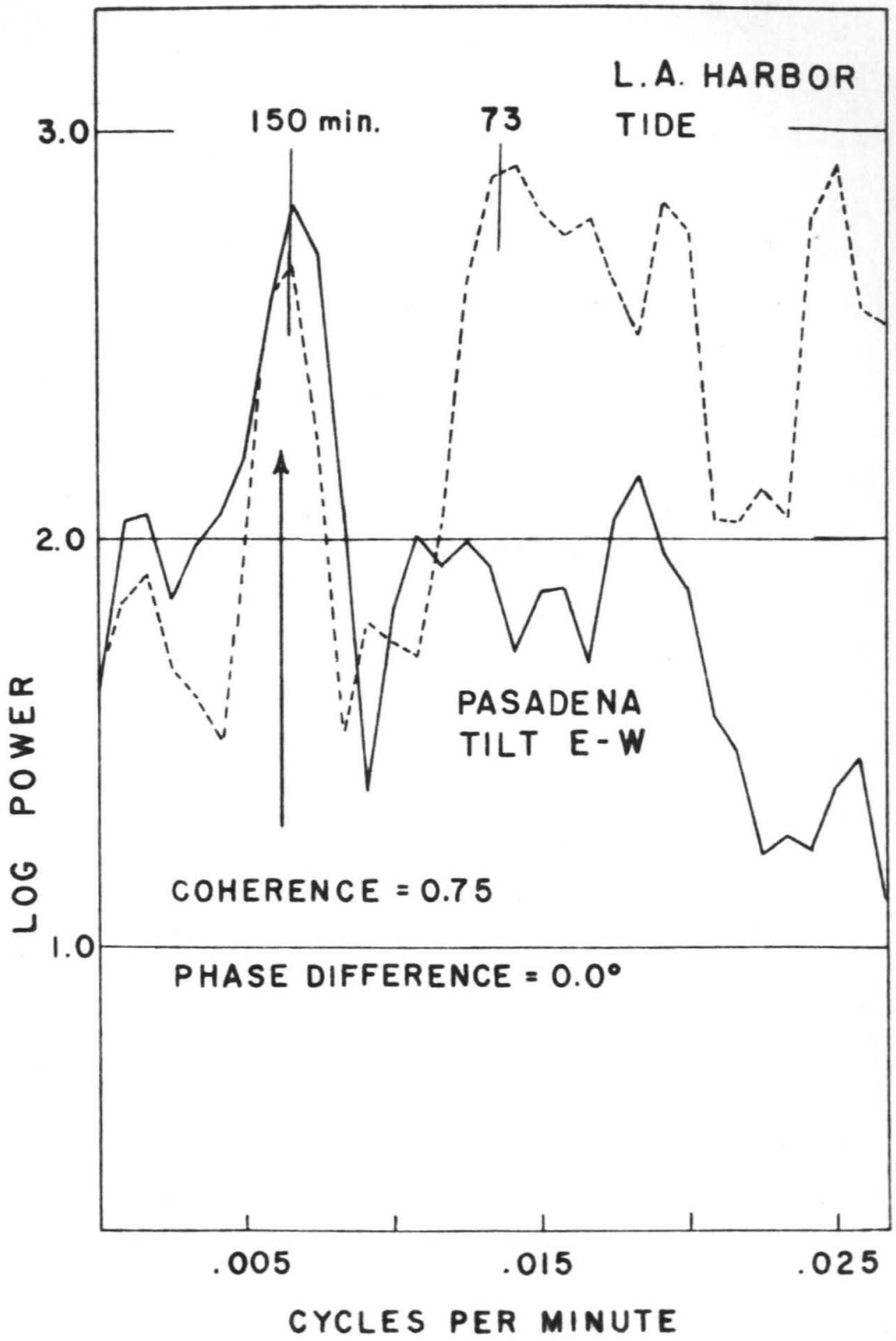
L.A. HARBOR
TIDE
150 min.
73
3.0
2.0
1.0
LOG POWER
PASADENA
TILT E-W
COHERENCE = 0.75
PHASE DIFFERENCE = 0.0°
.005
.015
.025
CYCLES PER MINUTE

FIG. 22

APPENDIX

Spectral Analysis Programs

Two separate data processing systems have been written in Fortran II for use on an IBM 7090. These programs have been written with enough generality so that they will handle any number of data points, and will read data in any BCD format from cards or magnetic tape. One group of programs is for performing cross spectral analysis on two sets of data, and the other is for Fourier analysis (periodogram analysis).

Setting up these systems was greatly aided by the use of several subroutines made available by Bell Telephone Laboratories. The major portion of the power spectra system consists of subroutine COQUAD written by Ruth Weiss, which we have modified to handle a larger number of lags and to compute the phase for the complex cross spectrum. The input to this subroutine is first buffered through subroutine LOPDEC which we designed to read data in blocks of less than a thousand words from magnetic tape, lowpass filter, decimate, and store in memory. In this manner we are not limited to the size of the memory (32, 768) but can work with any number of data points if we are willing to filter and decimate. A typical Press-Ewing seismogram for the Chilean earthquake will have up to 40, 000 points if digitized at 2 second intervals. After this operation, the data is cycled through a lowpass, decimate, and highpass operation any number of times. Just before entering the power spectrum section, a mean or linear trend is removed. A flow sheet for this system is given in fig. A1.

Since handling of large quantities of data requires explicit labeling of all output, the first card of each data deck contains the format of the data, the number of data points, the time increment, and 48 columns of identifying information such as station, date, component, etc. This identifying information is printed on all output resulting from computations performed on this set of data.

The Fourier analysis system also reads and filters the data with subroutine LOPDEC, cycles through a bandpass and decimation scheme and removes a trend. The main part of this program is subroutine FOUIER which we designed to select a subset of points N to M from a set of data of up to 23, 000 points, and Fourier analyze it for a specified frequency range at any desired frequency increment. Before entering this routine, we have the option of applying any symmetric time window to the data from N to M by calling the subroutine WINDOW. The arbitrary coefficients are read from cards and fitted to the data by linear interpolation. The main block of filtered data is held on a special buffer tape during computation when the WINDOW subroutine is used. Each time that a new time range N to M is specified, this tape is read in to restore the correct values of the entire set of data. The system is set up in this manner for the specific task of examining a narrow region of the spectrum as a function of time. A flow sheet for this system is presented in fig. A2.

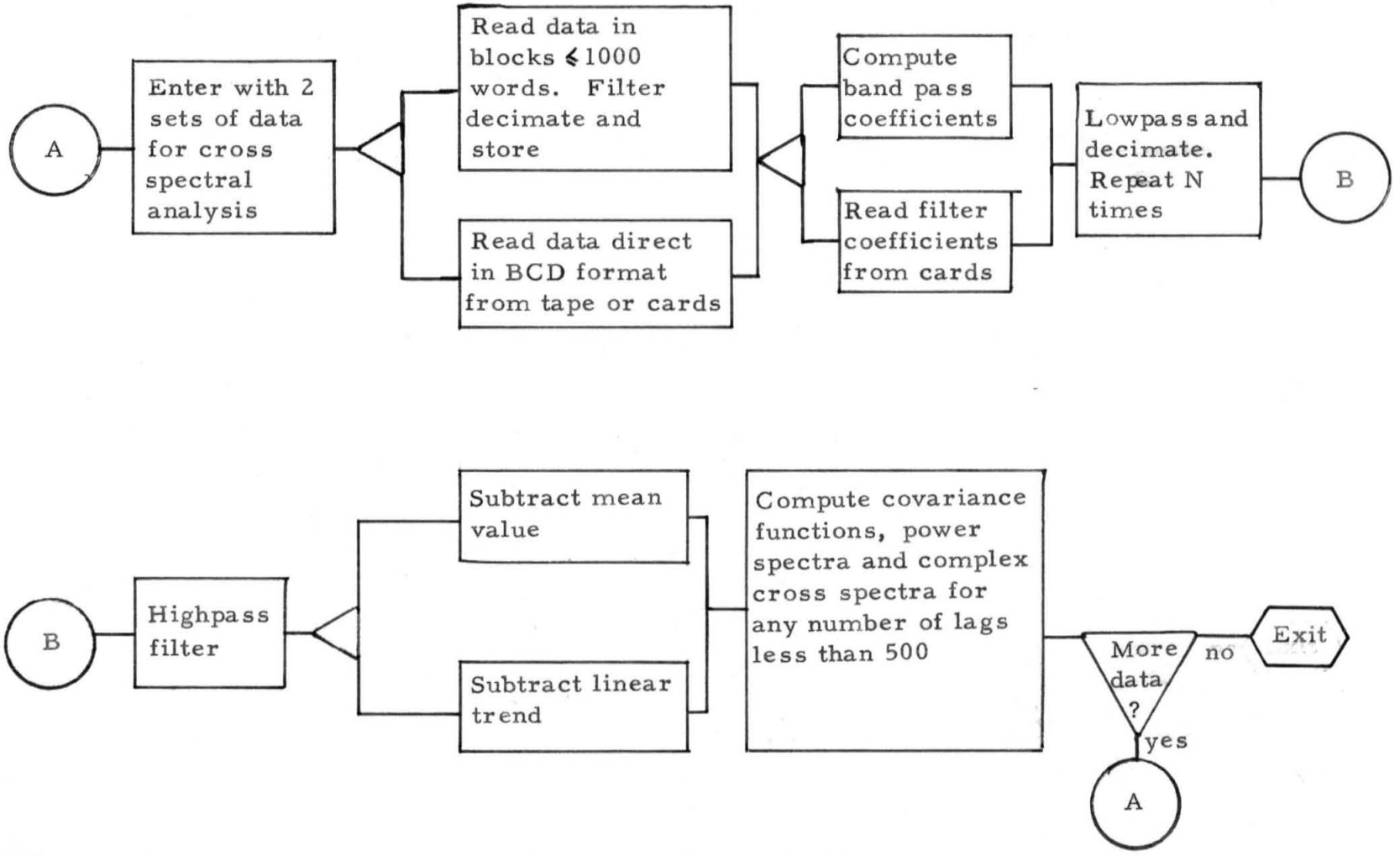

Figure A1. Flow Diagram for Power Spectral Analysis Program

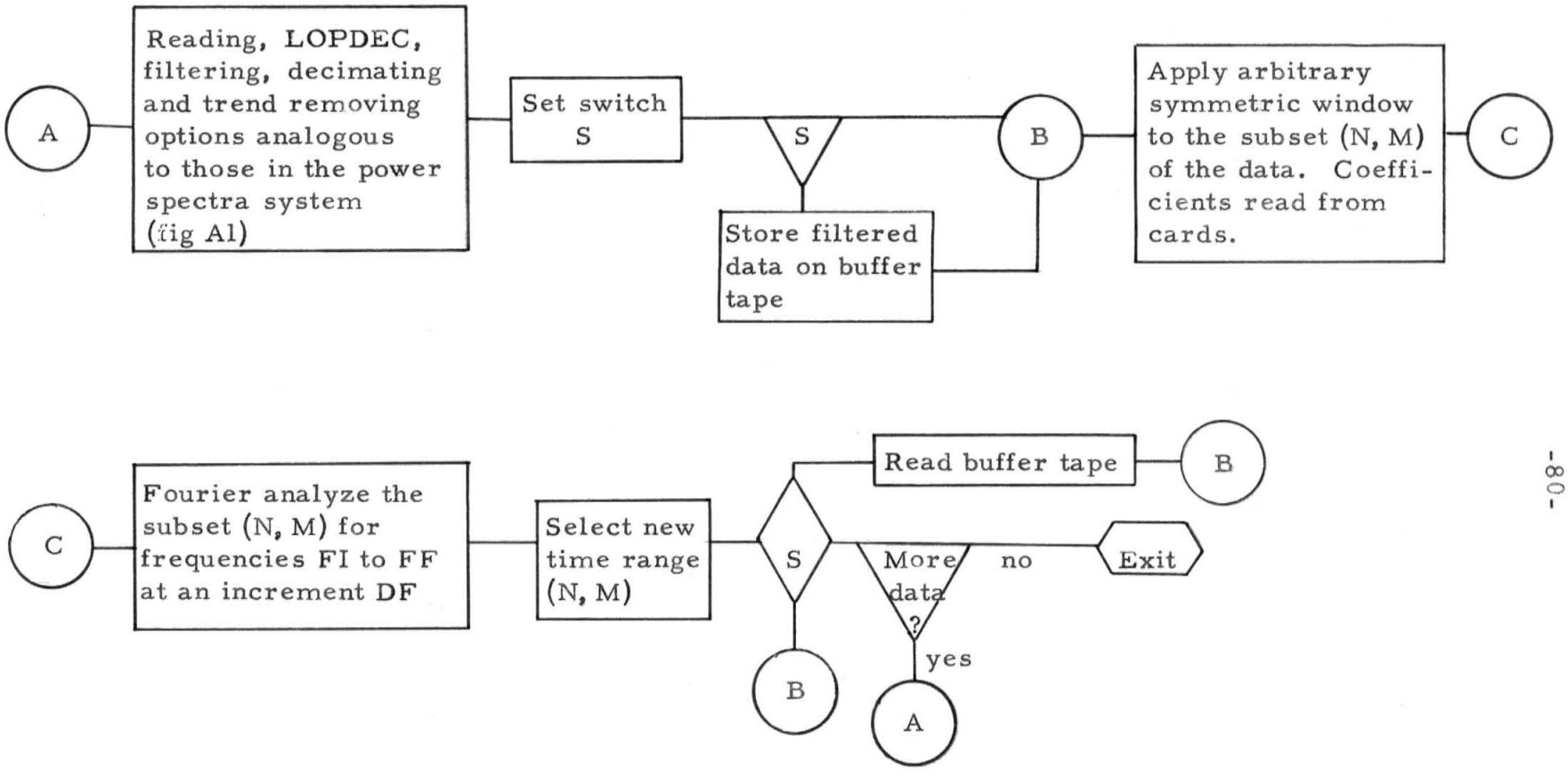

Fig. A2. Flow Diagram for Fourier Analysis System